Russian Geology and Geophysics © 2020, V.S. Sobolev IGM, Siberian Branch of the RAS
Vol. 61, No. 5–6, pp. 502–526, 2020 *DOI:10.15372/RGG2020102* *Geologiya i Geofizika*

Plate Tectonics vs. Plume Tectonics Interplay: Possible Models and Typical Cases

N.L. Dobretsov

Trofimuk Institute of Petroleum Geology and Geophysics, Siberian Branch of the Russian Academy of Sciences, pr. Akademika Koptyuga 3, Novosibirsk, 630090, Russia

Novosibirsk State University, ul. Pirogova 1, Novosibirsk, 630090, Russia

Received 16 October 2019; accepted 31 January 2020

The interplay of plume and plate tectonics is discussed with reference to well-documented late Paleozoic and Mesozoic–Cenozoic structures. The considered issues include models of lower mantle plumes; the typical case of the Hawaii plume; plate motions in the Pacific basin under the effect of plume activity and subduction processes; the role of plumes in the breakup of continents and rifting for the cases of the East African rifts and Gondwana breakup; large continental igneous provinces of Siberia and Tarim, with meimechites and kimberlites; and the formation of large granitic batholiths and related metallogeny. The study contains several points of novelty: integrated use of lower mantle seismic tomography and satellite altimetry data on gravity patterns; correlation of plume heat with plate velocities assuming that some plumes may dissolve in the asthenosphere; and correlation of rifting with compression and extension zones.

Keywords: Plate tectonics, plume tectonics, seismic tomography, gravity field, lower mantle, core, models of lower mantle plumes, plume magmatism, compression, extension

INTRODUCTION

Plate tectonics based on data from oceans on sea floor spreading, transform faulting, and subduction superseded the theory of geosynclines in the 1960s (Le Pichon, 1968; Coleman, 1977; Cox and Hart, 1986; Le Pichon et al., 1997; Bercovici, 2003). The plate tectonic ideas in Russia were spread due to a number of key publications since the 1970s (Sorokhtin, 1974; Zonenshain et al., 1976, 1990; Artyushkov, 1993; Zonenshain and Kuzmin, 1983, 1993). Later plate tectonics became extended by plume tectonics. The term was introduced by Maruyama (1994) who defined plume tectonics as referring to hot spots associated with mantle plumes that control global geodynamics. The hot spot concept belongs to Wilson (1965) who first applied it to the Hawaiian plume, while Morgan (1971) hypothesized that hot spots could represent melts ascending from a lower mantle source located below the convecting asthenosphere, most likely from the double (D_2) layer at the core-mantle boundary. The hypothesis received the first seismic tomographic proof for the Hawaii and Iceland plumes (Zhao, 2004). Data on past and present mantle plumes have been reported in several exhaustive overviews published in two recent decades (Pirajno, 2000; Abbot and Isley, 2002b; Ernst, 2014).

✉ Corresponding author.
E-mail address: DobretsovNL@ipgg.sbras.ru (N.L. Dobretsov)

Mantle geodynamics can be modeled at two levels: (i) plate tectonics represents plate motion which is driven by convection in the asthenosphere and is responsible for the events of opening and closure of oceans, subduction, and collision, with subsequent formation of orogenic belts; (ii) plume tectonics is related to ascent of material from the core-mantle boundary and accounts for global evolution trends and cycles (Dobretsov, 1980, 2010; Dobretsov and Kirdyashkin, 1994; Dobretsov et al., 2001). Yet, the interplay of plate and plume tectonics remains insufficiently understood.

This study bridges some gaps by considering the effect of plumes on rifting, petroleum potential, collisions, magmatism, and metallogeny. Some relevant problems were discussed at the 7th International Conference on Large Igneous Provinces (LIP-19, Tomsk, September 2019) coordinated by Richard Ernst, with participation of the author, namely: (1) role of plumes in continent breakup and evolution of oceans (section chaired by N. Dobretsov); (2) effect of plumes on climate and biospheric crises; (3) large igneous provinces and related metallogeny; (4) rifting and petroleum potential; (5) extraterrestrial planetary aspects (plumes on Venus, Mars, and Moon).

The problems discussed in this paper are:

1. General correlation between plate motions and plume activity (Figs. 1–6; Table 1).

2. Models of lower mantle plumes, including (a) boundary conditions and the role of the D_2 layer; (b) reactions at

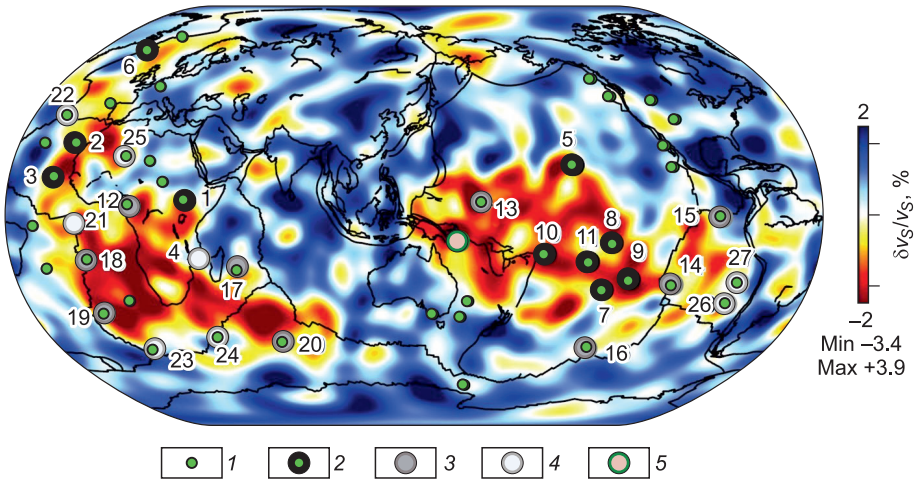

Fig. 1. Seismic tomography of the D_2 layer in the lower mantle at a depth of 2800 km, model SEMUCB-WM1 (Romanowicz et al., 2018). Scale on the right shows shear velocity (v_S) anomalies. *1*, all plumes and plume projections; *2–5*, primary (*2*), prominent (*3*), and poorly detectable (*4*) plumes, and those not related with hot spots (*5*).

the core-D_2 boundary, plume origin and velocity of ascending material; (c) spread of the plume head and LIP sizes (Fig. 7*a*,*b*; Tables 2 and 3).

3. Hawaiian plume, Pacific plate motions, and effect of plumes and subduction (Figs. 8–10).

4. Role of plumes in continent breakup, rifting, and origin of LIPs (Figs. 11–13).

5. Plumes under stable plates and collision zones; history of granite batholiths (Figs. 14–18).

PLATE TECTONICS AND PLUME TECTONICS: GENERAL BACKGROUND

Many of currently active and Cenozoic plumes are rooted at the core-mantle boundary (Fig. 1). Seismic tomography of the D_2 layer (Romanowicz et al., 2008; French and Romanowicz, 2015), with projections of modern and Cenozoic plumes (primary and prominent plumes 1–11, group I, and poorly detectable plumes 12–20, group II), shows two domains of slow shear-wave velocities or negative $\delta v_S/v_S$ ratios (Fig. 1). One in the area of the previously distinguished African hot spots (Zonenshain and Kuzmin, 1983, 1993) extends from the Iceland plume (6) in the north, through the African plume (1, 2, 3, 4), to the Kerguelen plume (20) in the Indian ocean. The other is located in the central and southwestern Pacific and comprises the Hawaiian (5), Pitcairn, Samoa, Tahiti (9, 10, 11), Macdonald (7), and Marquess (8) plumes. The two domains are referred to (Torsvik and Cocks, 2017) as the Tuzo (African) and Jason (Pacific) provinces. Their concentric structure, with fields of zero $\delta v_S/v_S$ ratios in the center surrounded by zones of negative anomalies on the background of positive $\delta v_S/v_S$, may record the convection pattern in the D_0 layer.

The pattern of $\delta v_S/v_S$ anomalies is presented in Fig. 2 in two W—E and four N—S crust and mantle profiles at different depths, with nearly vertical columns of negative ($-\delta v_S/v_S$) ratios corresponding to plumes of the two groups: Samoa (Fig. 2*a*), Samoa, Tahiti, Marquess (Fig. 2*b*), Pitcairn (Fig. 2*c*), Macdonald (Fig. 2*d*), Cabo Verde (Fig. 2*e*), Canary, and Iceland (Fig. 2*f*), as well as single or multiple local negative anomalies ($-\delta v_S/v_S$) beneath other plumes (unnamed circles) restricted to the upper mantle, without lower mantle roots. Thus, the clearly detectable primary plumes of group I are shown as symbols 2, 3 in Fig. 1 and as triangles in Fig. 2, while the poorly detectable features of group II are symbols 4, 5 in Fig. 1 and circles in Fig. 2 (see Table 1 for the complete list of plumes). The plumes of group I are connected with the layer D_2 and have high $^3He/^4He$ ratios (Table 1), high rank and buoyancy (Courtillot et al., 2003), while those of group II are poorly connected with layer D_2, have low $^3He/^4He$ ratios (except for three plumes with high $^3He/^4He$, Table 1), low ranks (0-1, or rarely 2), and low buoyancy (≤1.6, Table 1).

The group II plumes, which include more than 50% of modern plumes (Fig. 1; Table 1) differ in origin settings. Some (Ascension, Bouvet, Crozet) are located near mid-ocean ridges where their conduits could break down by mantle upwelling, but many plumes of group I (Iceland, Galapagos, Tristan, and St. Helena), which are likewise proximal to mid-ocean ridges, still keep connection (though poorly) with D_2 (Fig. 2*f*; Table 1). Plumes may lose their D_2 and core roots upon mixing with asthenosphere, especially near the upwelling axis, as detected in the case of the Hawaii plume (Sobolev et al., 2007). Otherwise, some may transform at the lower-upper mantle boundary or near the asthenosphere base, possibly, because carbonatite melts rising from the lower mantle into the asthenosphere are subject to change (see below); further studies are required to find out where and how it happens.

The relation of plumes with the core can be inferred from high $^3He/^4He$, PGE and Os isotope values (Hanski, 2004;

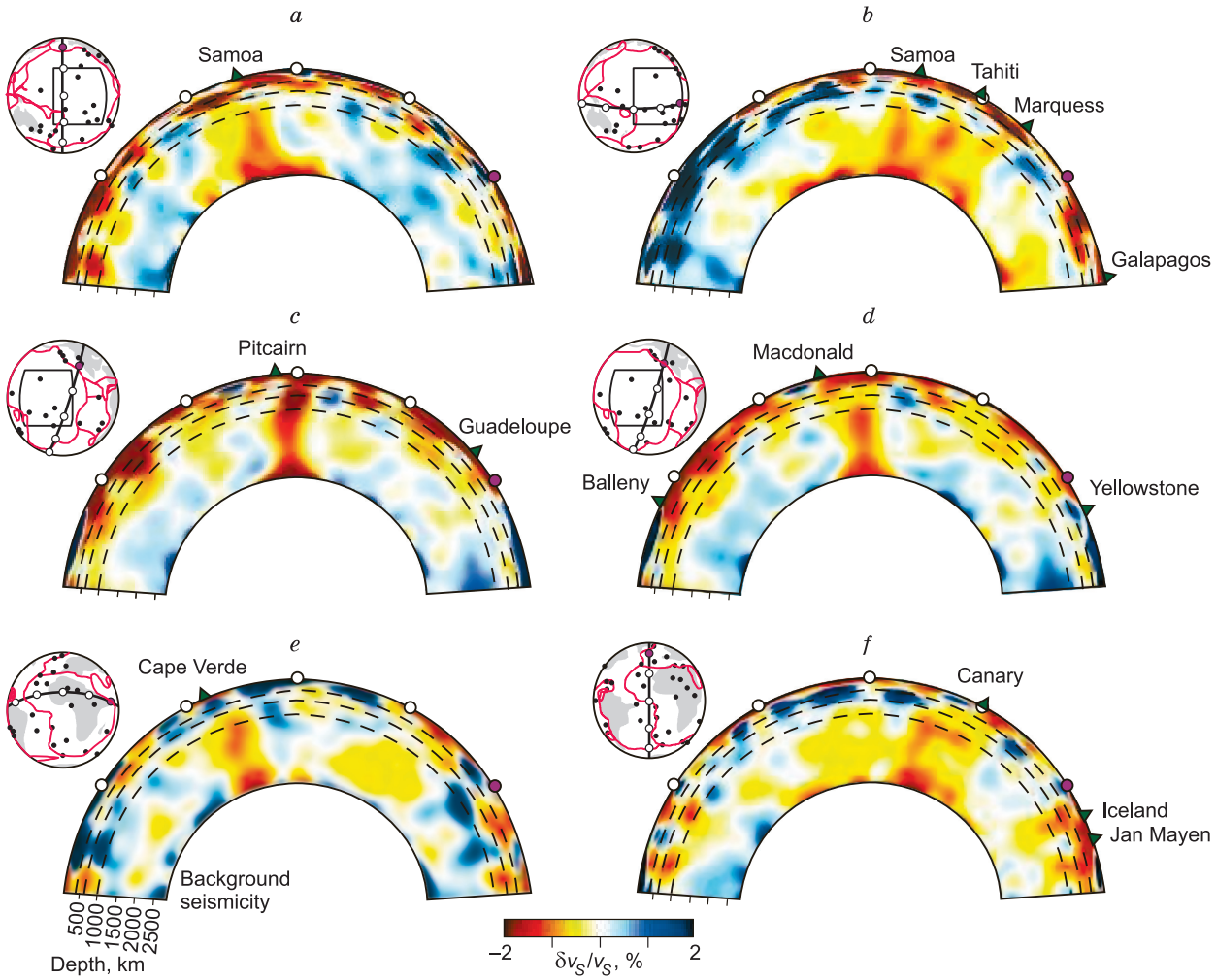

Fig. 2. Whole-mantle seismic images, with negative *P* velocity (v_P) anomalies in model SEMUCB-WM1 near main hot spots (French and Romanowicz, 2015). *a–f*: see text for description. Left top diagrams near each profile in *a–f* show their surface positions on the globe (Table 1).

Izokh et al., 2016), and from negative correlation of plume magmatism with the frequency of geomagnetic polarity reversals (Fig. 4). High $^3He/^4He$ is the most reliable indicator as $^3He^+$ generation is possible only in the core. The $^3He/^4He$ ratios are the highest in the Iceland, Hawaii (Loihi Island), and Reunion (Indian Ocean) plumes and sometime high in MORB (Fig. 3). As for the correlation with polarity reversals (Larson and Olson, 1991; Coffin and Eldholm, 1994; Dobretsov and Kirdyashkin, 1994; Condie, 2004), the plume-related eruption volume culminated (up to 10×10^6 km^3/myr) between 90 and 125 Ma when the polarity remained stable (86–124 Ma) but reduced to 1–2 $\times$ 10^6 km^3/myr in the time span when 4–6 reversals occurred per 1 myr (Fig. 4). The reason may be that heat withdrawal by plumes leads to core cooling, slow-down of convection, and cessation of reversals.

The convection pattern in a three-layer Earth model including the asthenosphere, lower mantle, and outer core layers (Fig. 5) shows flat (1:10 to 1:100) and stable cells in the asthenosphere, at a high temperature gradient along the lower-upper mantle boundary (Kirdyashkin and Dobretsov, 1991; Kirdyashkin et al., 1994; Dobretsov et al., 2001), slow and unstable convection in the lower mantle, which stabilizes after reduction of plume activity (Kirdyashkin and Dobretsov, 1991; Kirdyashkin et al., 1994; Dobretsov et al., 2001), and intense highly turbulent convection in the outer core. The core convection is controlled by heat evacuation with plumes, and greater turbulence correlates with increasing frequency of geomagnetic reversals (Larson and Olson, 1991; Kirdyashkin et al., 2000; Dobretsov et al., 2001). Convection is especially intense beneath thick parts of D_2 (Fig. 5*b*) which correspond to the African and Pacific plumes (low v_S) and to the respective Tuzo and Jason provinces: for the intervals 200–300 Ma in Fig. 5*a* and 145–300 Ma in Fig. 5*c*.

Panel *a* in Fig. 5 shows LIPs and kimberlites localized in the Tuzo and Jason provinces and in their surroundings on continents, while the 200–300 Ma oceanic crust has not preserved. The space between the Tuzo and Jason provinces accommodates zones of subduction (Fig. 5*c*). The geoid surface is uplifted above the African and Pacific plumes (dash

Table 1. Plumes of groups I and II (Romanowicz and French, 2018)

No.	Plume ID	Rank (Courtillot et al., 2003)	Buoyancy	$^3He/^4He$
1	Afar	4	1	High
2	Tanzania			High
3	Canary	2	1	Low?
4	Cabo Verde	2	1.6	High
5	Hawaii	4+	8.7	High
6	Iceland	4+	1.4	High
7	Mcdonald	2+	3.3	High?
8	Marquess	2+	3.3	Low
9	Pitcairn	2+	3.3	High?
10	Samoa	4	1.6	High
11	Tahiti/Society	2+	3.3	High?
12	Cameroon	0+	2	High?
13	Caroline	3	2	High
14	Easter	4+	3	High
15	Galapagos	2+	1	High
16	Louisville	3+	0.9	High?
17	Reunion	4	1.9	High
18	St. Helena	1	0.5	Low
19	Tristan	3	1.7	Low
20	Kerguelen	2+	0.5	High
21	Ascension	0+	1	?
22	Azores	1+	1.1	High?
23	Bouvet	1+	0.4	High
24	Crozet	0+	0.5	?
25	Hoggar	1	0.9	?
26	Juan Fernandez	2+	1.6	High
27	San Felix	1+	1.6	?
28	Indonesia	–	–	Low
and other 17 hot sports of unknown nature				

line in Fig. 5*b*) in the reconstruction of Torsvik and Cocks (2017), though the geoid anomalies are not associated with the Tuzo and Jason provinces in the satellite Gravity Recovery And Climate Experiment *(GRACE*) model.

Although many issues of lower mantle and outer core convection are unclear, the available empirical data (Figs. 1–5) confirm that plumes control the heat and mass transfer across the core-mantle boundary (see below).

The relative importance of plate and plume tectonics correlates with plate velocities. Plate tectonics predominates in fast plates where plumes have poor surface record though they heat up the asthenosphere and induce plate acceleration, while plume tectonics is more important and diverse in he case of slow spreading plates. The velocities of plates can be estimated either from the NUVEL model or from a global model assuming friction coefficients of 0.03 (3%) at convergent boundaries and 0.1 (10%) at divergent and transform boundaries (Sobolev and Brown, 2019). The estimates obtained with the two models are similar, except for some discrepancy in Eurasia. Fast plates cover about 50% of the surface (Fig. 6) and are surrounded by zones of plate interactions: (i) circum-Pacific Cordilleran-type collision and subduction in the east and island arc subduction in the west and northwest, from Alaska to New Zealand, and (ii) the Himalaya-Alpine collision northwest of the India-Australia plate. Subduction was hypothesized to control the velocity and evolution of plates due to entrained sediments that would act as lubrication (Sobolev and Brown, 2019), but the idea was met with criticism (Behr and Becker, 2018; Behr, 2019) and has been open to discussion. Plate motions in the zones of interactions are especially fast and accompanied by seismicity. The modern circum-Pacific subduction zone mimics the seismicity belt in Fig. 5*c*, where seismic areas fall outside the Tuzo and Jason provinces. The zones of subduction and sinking in the lower mantle (Fig. 5*b*) are likewise located between the Pacific and African LLSVP areas, i.e., the anomalies in the D_0 layer do not interact with subduction zones and downwelling, which is determined by mantle geodynamics. Some models predict that material stacked beneath subduction zones may form zones of melting in the D_0 layer.

Therefore, plumes in backarc basins (Yarmolyuk et al., 2013; Kuzmin et al., 2018) hardly can be abundant, but the problem of subduction zones and diversity of their structure, especially, with the backarc setting, is still challenging (Bogdanov and Dobretsov, 2001; Dobretsov, 2011).

MODELS OF LOWER MANTLE PLUMES

The model discussed in this section was described in previous publications (Dobretsov et al., 1993, 2001; Dobretsov and Kirdyashkin, 1994; Kirdyashkin et al., 1994). It generally agrees with many other models (Ernst, 2014). Possibly, scientists will arrive at a universal plume model some day.

Plumes can be purely thermal that melt the ambient mantle, purely compositional that differ in density from the ambient mantle due to enrichment in some fluid or melt components, or mixed in which some volatile chemical dope decreases the melting temperature of the ambient mantle. Yet, it is hard to identify the plume nature from their surface manifestations (Dobretsov et al., 1993, 2001).

Experimental studies for different models show that a channel- or a flare-like melting zone can form above a local heat source with its melting temperature exceeding that of the ambient mantle ($T > T_{mlt}$) or above a source of volatiles that can lower the ambient melting temperature (Dobretsov et al., 2001, 2010; Dobretsov, 2010). According to the model of a mixed thermochemical plume, with starting and boundary conditions as specified previously (Dobretsov et al., 1993, 2001; Dobretsov and Kirdyashkin, 1994; Dobretsov, 2008), the temperature excess at D_2 over the average at the core boundary (T_1 relative to T_0) consists of two intervals:

$$\Delta T_0 = T_{mcd} - T_0 \sim 400\ ^\circ C, \quad (1)$$

$$\Delta T_1 = T_1 - T_{mcd} = kC_2 \sim 0.3\ \Delta T_0,\ \Delta T_2 = T_{md} - T_1, \quad (2)$$

where T_{mcd} is the melting temperature of the mantle substrate with a chemical (volatile) dope; T_{md} is the melting temperature of the dry substrate; C_2 is the dope concentra-

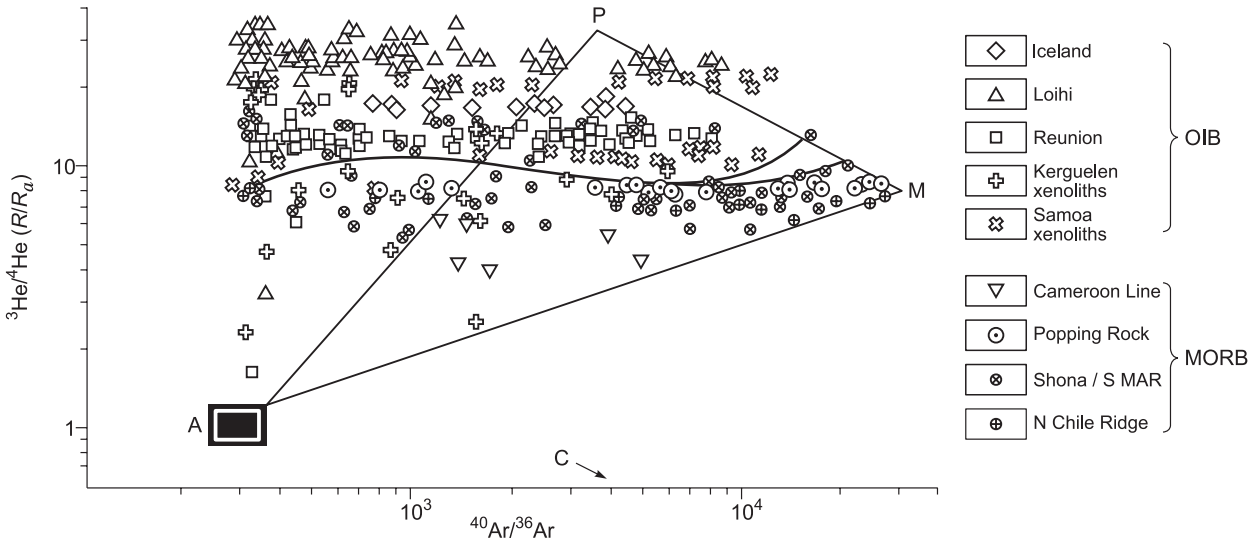

Fig. 3. He-Ar isotope systematics of volcanics from mantle plumes (P, OIB) and mid-ocean ridges (MORB), modified after (Graham et al., 1992; Kurz and Geist, 1999; Schilling et al., 1999). Average and characteristic compositions: A, atmosphere; C, continental crust; M, mantle; P, plumes. R/R_a denotes ^{3}He/^{4}He ratios relative to the atmospheric standard.

tion in the plume head; K is the coefficient of melting temperature decrease due to the volatile component. The 100 °C decrease requires at least C_2 = 3% and K ~30 for an H_2O dope and C_2 ~ 10% and K ~ 10 at predominant CO_2. The position of T_1 between T_{mcd} and T_{md}, crucial for modeling, depends on the dope composition and controls the amount of heat in the plume.

The thermochemical plume in the model of Fig. 7*a* results from reactions in the fluid mixture released at the core-mantle boundary. The outer core melt consisting mainly of Fe^0 can release only reduced gases (three main components in the first approximation): hydrogen, methane and possibly other hydrocarbons, and hydrides of metals (Dobretsov et al., 2001; Litasov and Shatsky, 2016), including also hydrides of K, Na, Li and Si since magmas found in plume-related eruptions are always silicic and K-rich (occasionally with carbonatite); melts in the lower mantle may be carbonatitic.

In this case, the simplified reaction is (Fig. 7*a*)

$$\underbrace{H_2 + CH_4 + SiH_4 + 2KH}_{\text{Core fluid}} + \underbrace{11FeO}_{\text{Lower mantle component}} \rightarrow$$

$$\rightarrow \underbrace{6\,H_2O\uparrow + CO_2\uparrow + SiO_2\uparrow + K_2O\uparrow}_{\text{Plume melt}} + \underbrace{11\,Fe^0\downarrow}_{\text{Core melt}}$$

Oxidation in this reaction is provided by oxygen from FeO (magnesiowüstite, (Mg, FeO)) and other iron-bearing phases at D_2. At sufficient FeO inputs, the reaction shifts to the right, with the formation of Fe^0 that sinks into the core and high-melting components (H_2O, CO_2, SiO_2, K_2O, etc.) that dissolve in the melt and rise into the forming plume conduit. The additional input of iron into the core can be confirmed by proving that core became larger and heavier after the accretion.

The stability of the plume conduit in the lower mantle depends on its heating power and the ambient mantle properties. At low heat, the plume may become discontinuous and spin until complete collapse (Dobretsov et al., 2001). The amount of heat N (thermal energy) depends on ΔT_0 at the core boundary, plume conduit diameter d_k and mantle properties (thermal conductivity λ_p, thermal expansion β, diffusivity α, and melt viscosity ν). The equation is (Dobretsov et al., 2001):

$$N = 0.025\,(\pi d_k^2\,\lambda_p \Delta T_0^{4/3})\,(\beta g/\alpha\nu)^{1/3}. \quad (3)$$

At the heat N, the thermal energy Ndt is spent on melting a conduit of the diameter d_k to the height dx:

$$Ndt = 1/4\pi\rho d_k^2\,(B + C\Delta T_0)dx, \quad (4)$$

where B is the heat melting and C is the heat capacity.

Equation (4) allows estimating the rate (dx/dt) and time (t) of melting. The time is 2.7 to 4.8 myr depending on temperature and thermal energy, for Δx = 2900 km (see Table 2 for parameters of plumes 100 and 70 km in diameter and the time t = 2.7–4.8 myr). This time is sufficient for correlating the total amount of mantle material rising from the core to the surface with the frequency of geomagnetic reversals (Fig. 4) (Dobretsov et al., 2001; Kirdyashkin et al., 2001).

A plume head spreading for the time t_1–t_3 when impinged on the base of a low-melting dunite-harzburgite lithosphere of the thickness $x_2 = H - x_1$ is enlarged in Fig. 7, *b*. The time t_3 depends on the growth time of a Δx_p high secondary plume till the formation of a dike system and voluminous eruptions of lavas. Thus, the time t_3 can be different, but it defines (at a given plume thickness) the sizes of the plume

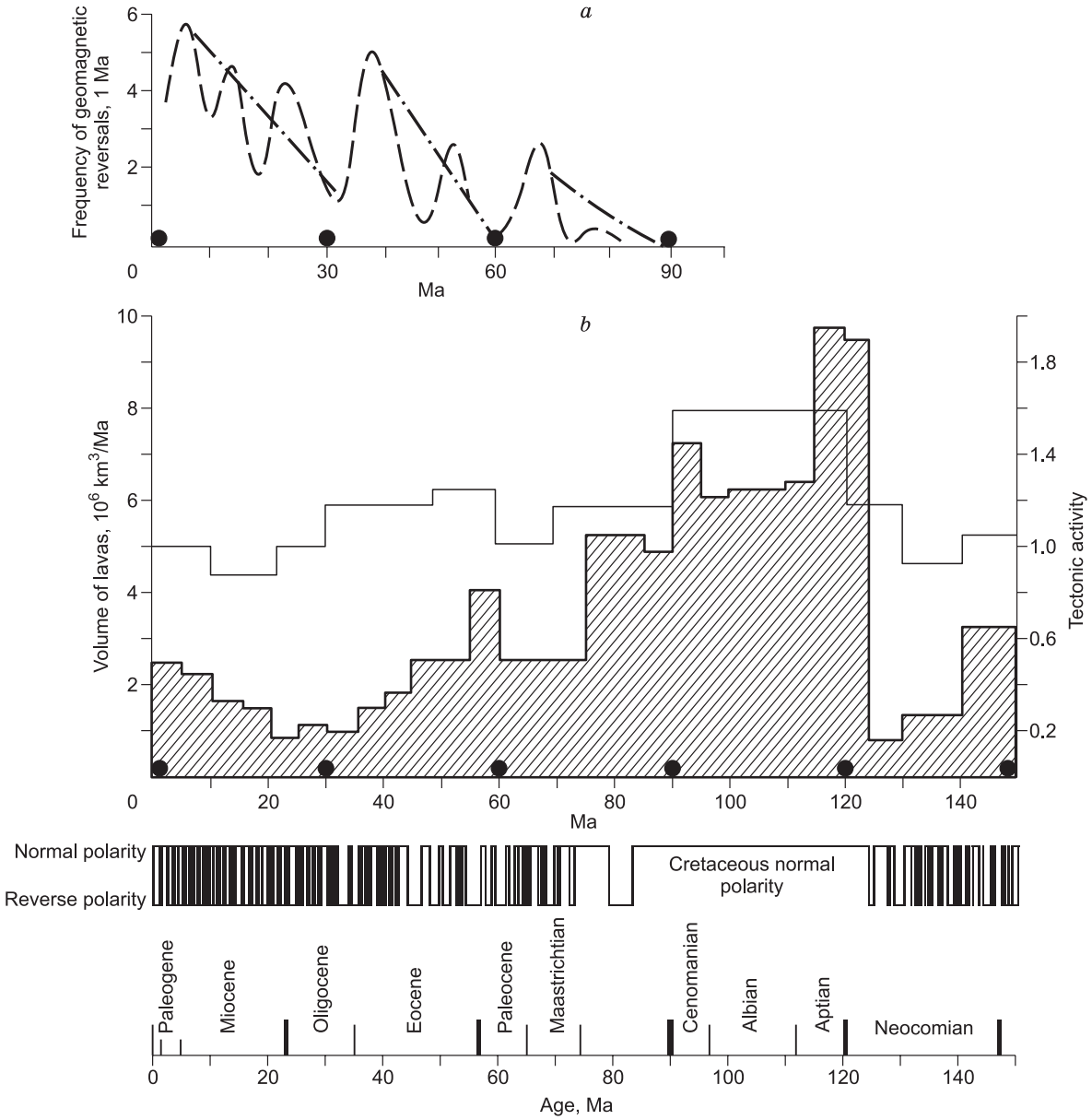

Fig. 4. Frequency of geomagnetic reversals (Mazaud and Laj, 1991) (*a*), peaks of mantle magmatism correlated with stable normal polarity interval (90–120 Ma) and decreasing peaks with increasing frequency of reversals (Larson and Olson, 1991; Dobretsov and Kirdyashkin, 1994) (*b*); Tectonic activity, after (Zonenshain and Kuzmin, 1993). See text for explanations.

head and the related igneous province. The sizes of the plume head and the respective LIP as a function of the stored plume heat $N(w)$ were estimated previously, at the $L_{fr} = 0.5$ melt fraction in the plume head, for continental lithosphere at $x_2 = 200$ km and transitional lithosphere at $x_2 = 100$ km (Dobretsov et al., 2001; Dobretsov, 2008, 2011); correspondingly, the heights of the secondary plumes Δx_p can be about 130 and 30 km, respectively, and the respective time periods are 5.3 and 1.2 myr (Dobretsov, 2008; Dobretsov et al., 2013). For the Hawaii plume, the estimated LIP diameters are 600–700 km at $N(w) = 3 \cdot 10^8$ kW and the $x_2 = 100$ km thick transitional lithosphere; 300–350 km at $x_2 = 50$ km oceanic lithosphere, and as large as 1100–1400 km for continental lithosphere; for plumes as hot as $(1.2–1.3) \cdot 10^9$ kW, like those in Siberia, the size can increase to 3000–3500 km. Table 3 provides data on ten LIPs, from 3500 to 800 km, composed mainly of flood basalts, with the plume heat from $2.5 \cdot 10^9$ to $(3–4) \cdot 10^8$. Heat of some plumes in Table 3 was estimated from the specific volume of eruptions for the lack of data.

The model of a lens-shaped plume head (Fig. 7*b*) demonstrates that LIPs form in several stages: (1) initial rifting; eruptions of primary poorly fractionated melts; no large plume head; (2) large-scale eruptions of fractionated melts, mainly homogeneous tholeiites for flood basalts (60–80% of melts erupted for 0.5–1.0 myr for the Siberian trapps); (3)

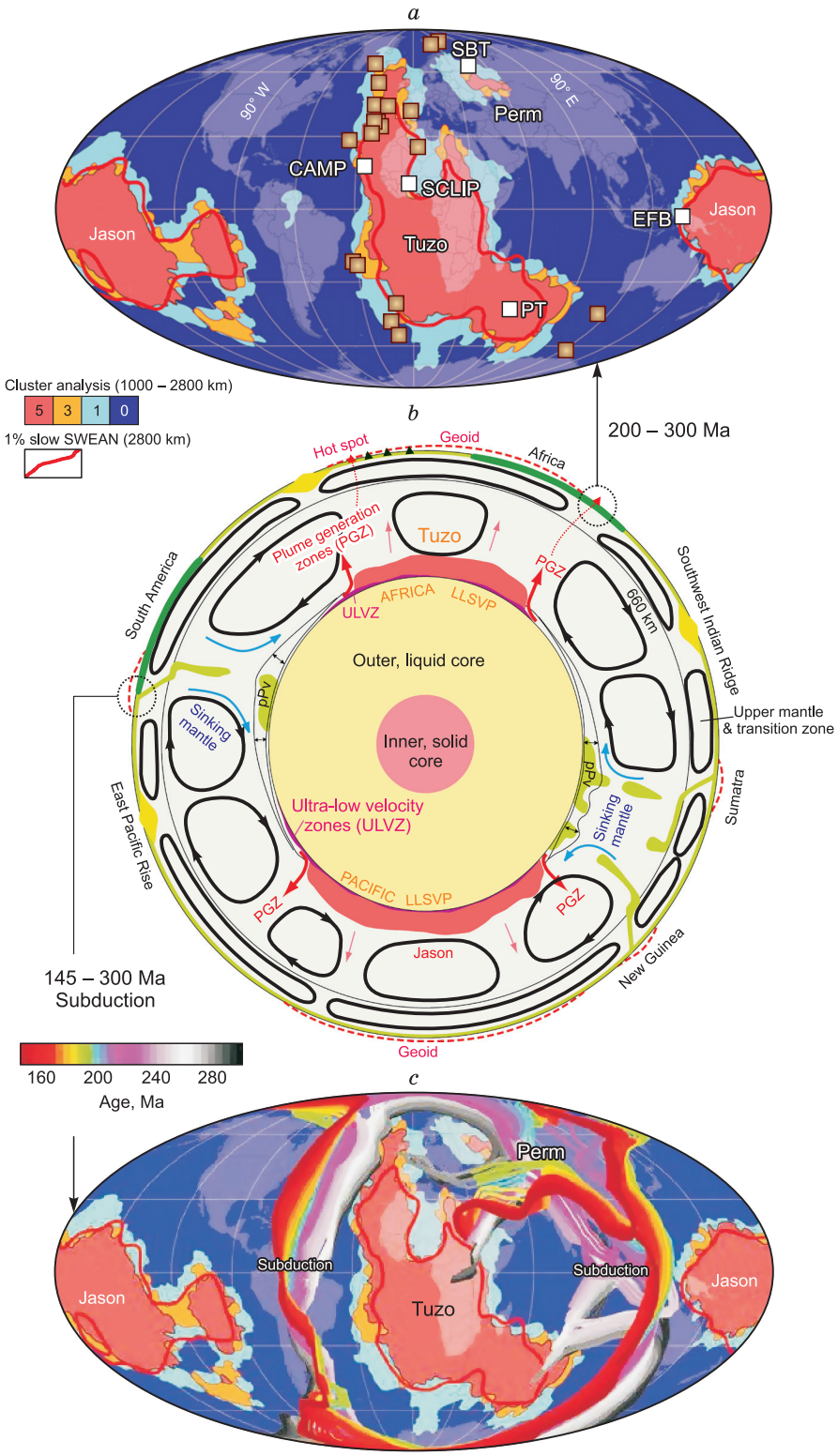

Fig. 5. Earth after Pangea, 200–300 Ma, modified after (Torsvik and Cocks, 2017). *a*, Zones with different concentrations of plumes and provinces of Jason and Tuzo, based on Fig. 1; SEMUCB (or SMEAN) models; LIPs (5 white squares) and kimberlite fields (47 brown squares), SBT, Siberian traps (continental flood basalts); NAMP, North American mantle plume; EFB, Emeishan flood basalts; *b*, cross section of the Earth with two-layer mantle convection and turbulent convection in the core; thick D_2 layer at the core boundary: African and Pacific plumes corresponding to Tuzo and Jason provinces, respectively; *c*, Earth after Pangea, 145–300 Ma, with Tuzo and Jason provinces and subduction between them. See text for explanations.

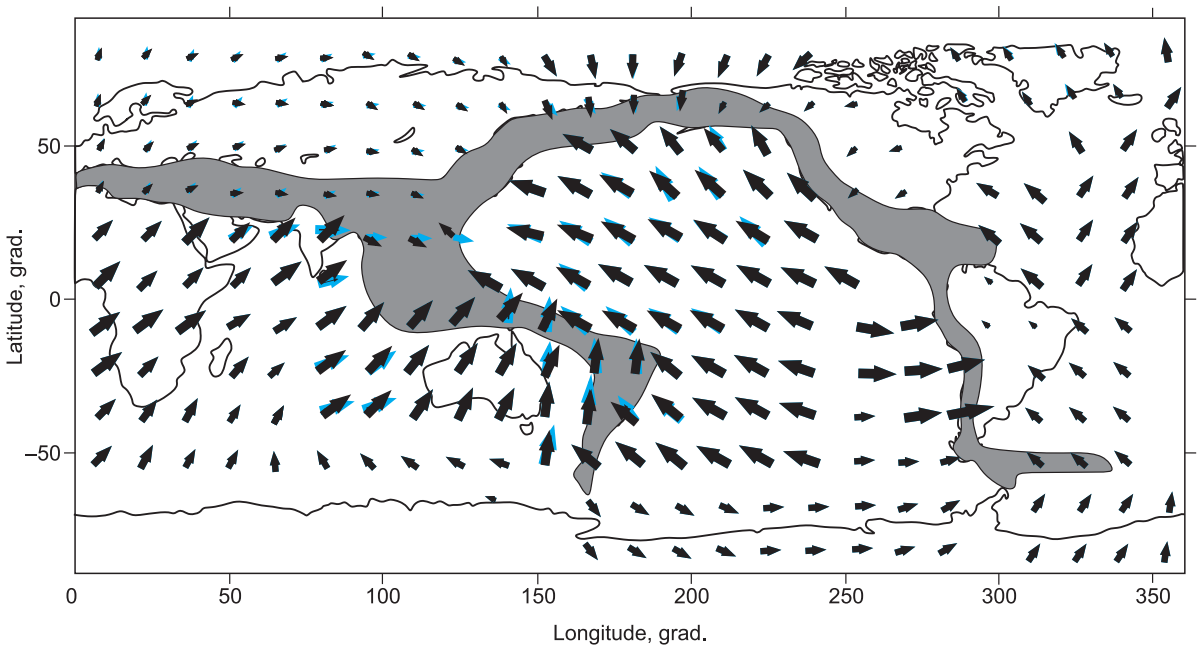

Fig. 6. Plate velocities (Sobolev and Brown, 2019) estimated using (i) NOVEL model (black arrows) and (ii) friction in subduction zones (blue arrows). Gray zone = interactions between fast plates.

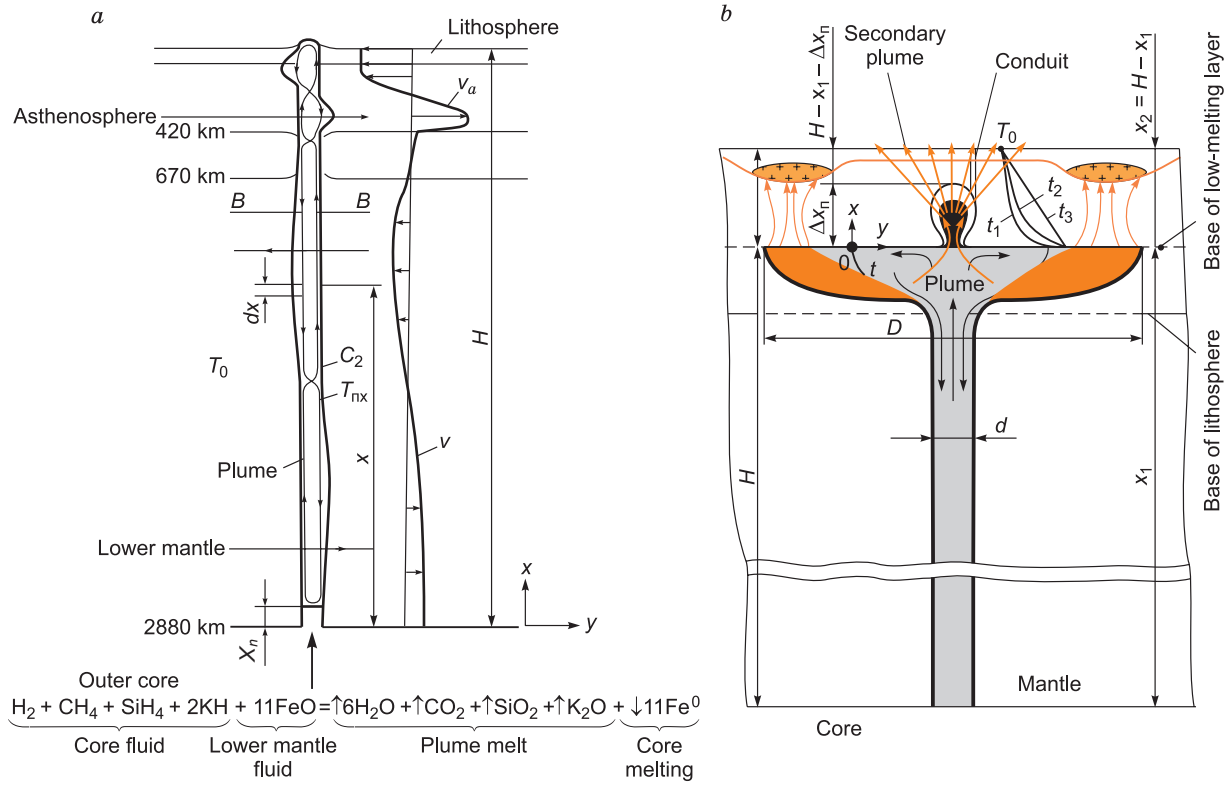

Fig. 7. Origin and ascent of plumes (Dobretsov et al., 2001, 2008). *a*, Plume rising to height *H* in the lower mantle, and effect of v_a mantle flow in astenosphere; x_n = height of molten core material and D_2 melting under flow of volatiles from the core; *b*, plume head under the lithospheric base uplifted by collapse of lithospheric blocks and their dissolution in the plume material; rise of Δx_n high secondary plume and a complex of radiated dikes above (red arrows above conduit); dikes withdraw material from most of magma chambers at the time t_3; granitic melt (crosses) under the effect of fluids (thin arrows). See text for explanations.

Table 2. Parameters of thermochemical plumes (Dobretsov, 2011)

d_s, km	C_2, %	C_1, %	$\Delta T_1 = T_1 - T_{mcd}$, °C	$\Delta T_0 = T_{md} - T_0$, °C	N, kW	t, Ma	u, m/yr
70	1.1	2.1	18.5	381	3.5×10^8	2.7	1.1
100	1.4	2.2	12	371	4.0×10^8	4.8	0.6

compositionally heterogeneous residual + additional melts; felsic melts (rhyolite or granite) produced by plume interaction with thick collisional crust containing batholiths (see below). Carbonatite alkaline magmatism and injections of dikes (Dobretsov et al., 2010) may follow but hardly can be interpreted as a separate stage (Dobretsov, 2010, 2013).

HAWAII PLUME AND PACIFIC PLATE MOTIONS

The Hawaii plume has been the best documented hotspot whose track (Fig. 8*a*) became a proof for the Pacific plate motion at the onset of the plate tectonic theory (Wilson, 1965; Morgan, 1971). The hotspot is still used as reference to update the relative plate motion while the structure and composition of the Hawaii volcanoes have implications for the composition of the source magma and its interaction with the asthenosphere (Fig. 8*b*). The Emperor chain of volcanoes was active between 80 and 45 Ma and produced voluminous ash eruptions marked by a prominent gravity low (Fig. 8*a*) commensurate with those in the Kamchatka-Aleutian trench filled with more than 2 km of sediments.

The N–S direction of the Pacific plate motion changed to WNW (~65°) at about 45 Ma. The change took about 2–3 myr, as indicated by a bend of the Emperor chain toward the Hawaiian one; ash eruptions stopped and then resumed partly for the past 10 myr. The data on the Emperor-Hawaiian volcanic chain (Fig. 8*a*) are best consistent at the assumption that all plumes, including the Hawaiian one, move southwestward with respect to stable Africa while the Pacific plate is rotating (Torsvik and Cocks, 2017). The same assumption of Africa as a reference frame for continuously moving long-lived plumes and their partial rotations, was used in reconstructions for the Paleozoic and Mesozoic eras (Torsvik and Cocks, 2017). The results place constraints on asthenospheric convection and contradict the idea of hot spots being the basic reference (Zonenshain and Kuzmin, 1983, 1993).

The position of the Hawaii Islands and the structure of the Hawaii plume (Fig. 8*b*) support the hypothesis that the plume undergoes partial rotation and allow estimating its diameter: a 80–120 km conduit and a 120–150 km head. These estimates agree with the above model, which predicts that the plume power $3\cdot10^8$ kW of heat. The percentages of primary mantle material in the plume (Sobolev et al., 2005, 2007) vary from ~40% in the center, 27% in the Mauna Loa crater, 12% in the Kilauea crater on the margin of the inner zone, to as little as 2% on the margin of the outer zone, in the Loihi seamount area (Fig. 8*b*). The corresponding estimates of magma temperatures are 1460 °C in the Loihi area, 1520 °C at Kilauea, 1600 °C at Mauna Loa, and 1660 °C in the plume center (Sobolev et al., 2005, 2007), which are 200 °C higher than for typical MORB.

As inferred from the lava compositions in the Mauna Loa and Kilauea craters and in the Loihi seamount, the plume melt prior to mixing with MORB-type melts in the asthenosphere was composed of ca. 23% MgO, 38% SiO_2, and

Table 3. Large igneous provinces for the past 300 years (Dobretsov, 2011)

Province, complex	Age of main (subsidiary) phase, Ma	Diameter, km	Heat*, kW	Reference
Tarim	280	2500	10^9	(Borisenko et al., 2006)
Siberian traps	250 (240)	3500	2.5×10^9	(Dobretsov, 2005)
Emeishan (China, Vietnam)	260 (250)	1500	10^9	(Hoa et al., 2008; Shellnutt, 2014)
Barents Sea	180 (200)	1500	6×10^8	(Dobretsov, 2005)
Central Atlantic	190 (205)	2000	6×10^8	(Pirajno, 2000)
Ferrara-Tasmania	175	1500	10^9	»
Okhotsk volcanic plateau	150	1500	10^9	(Bogdanov and Dobretsov, 2002)
Ontong Java, Pacific	122 (90)	2800	2×10^9	(Coffin and Eldholm, 1994)
Kerguelen, Indian ocean	115 (60)	1500	10^9	»
Broken Ridge, Indian ocean	90	1000	5×10^8	»
Caribbean plateau	90	1500	10^9	»
Deccan, India	60	1000	5×10^8	»
North Atlantic province	60	~2000	7×10^8	»
Ethiopian plateau	30 (15)	1500	5×10^8	»
Columbian plateau, USA	15	1000	5×10^8	(Pirajno, 2000)
Iceland	0-5	800	4×10^8	»

*Estimated from specific volume of eruptions

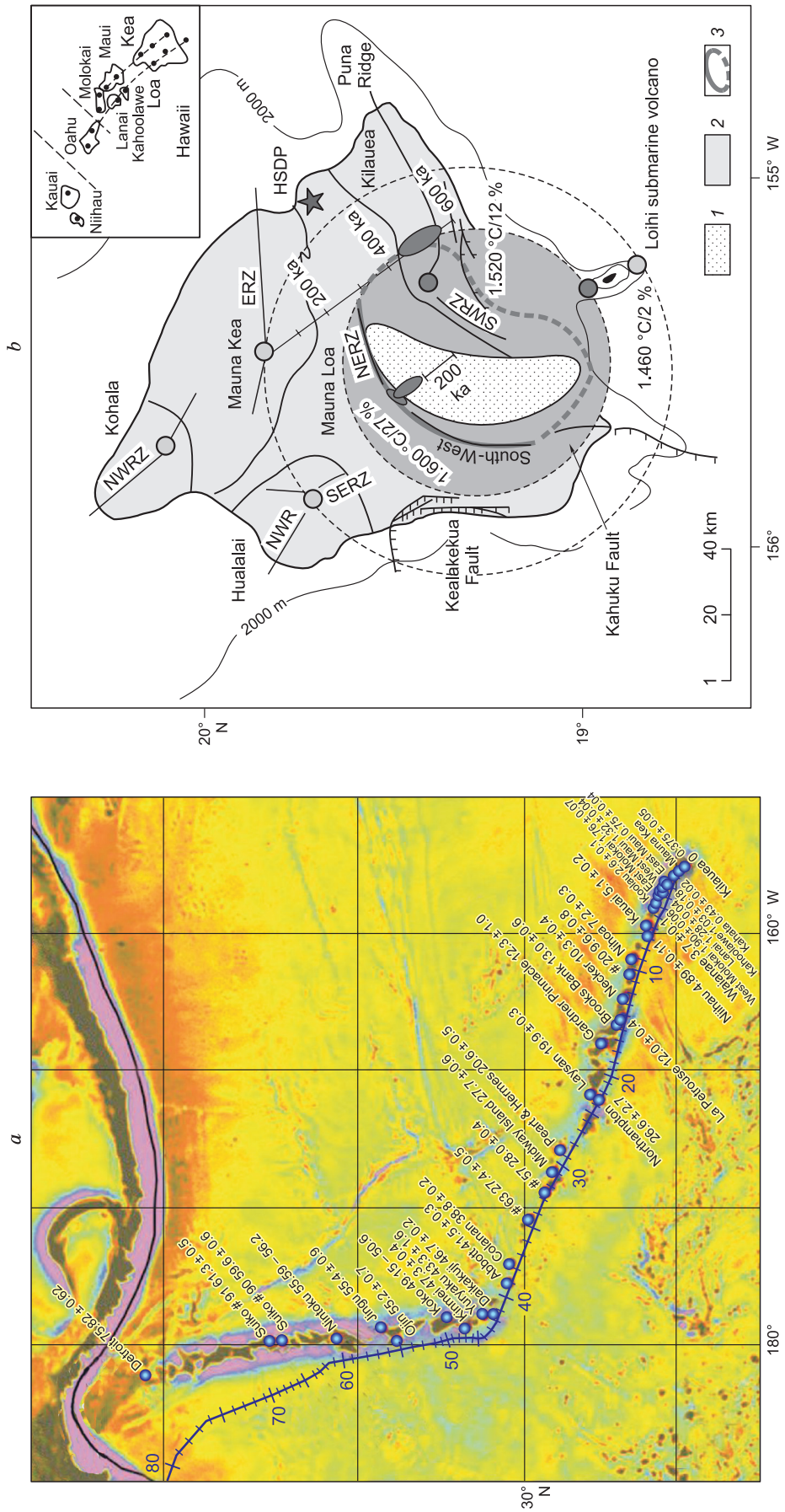

Fig. 8. Track of the Hawaii plume with ages of eruptions and calculated plate path on the background of gravity pattern in the northeastern Pacific (a); modern Hawaii plume and parameters of plume melt (*b*). *a*, Aleutian arc, zone of ash fallout around the Emperor chain of volcanoes, sea floor structure, after (Torsvik and Cocks, 2017); *b*, *1*, axis zone, till 200 km depth; *2*, central zone; *3*, narrowing of central zone at 170 km depth (Sobolev et al., 2005). See text for explanations.

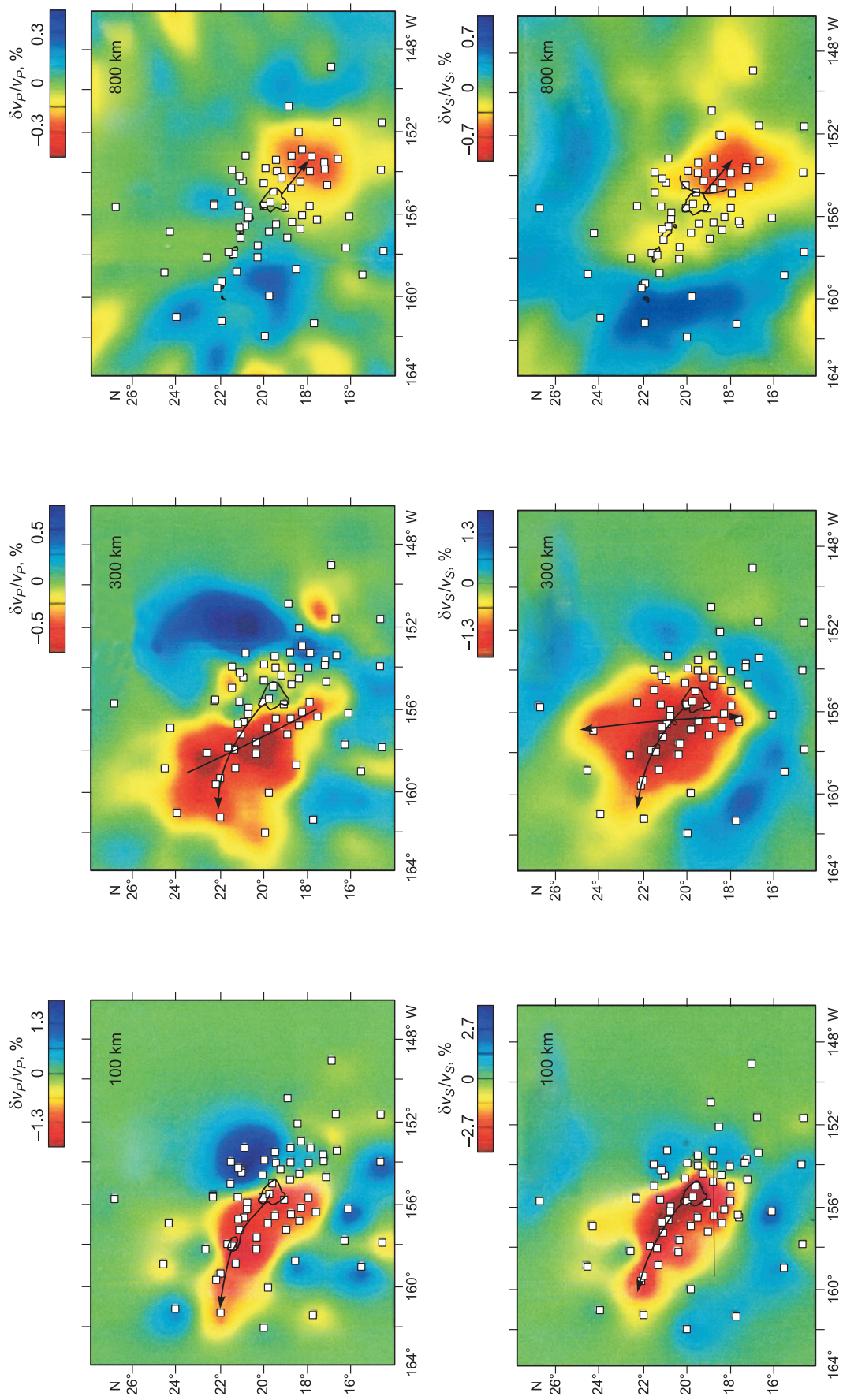

Fig. 9. *P*- and *S*-wave seismic tomography of the Hawaii plume, slices at depths 100, 300 and 800 km (Laske et al., 2009; Wolfe et al., 2009). Black line contours Hawaii Island (Fig. 8*b*); arrows are directions of plume and mantle material (300 km).

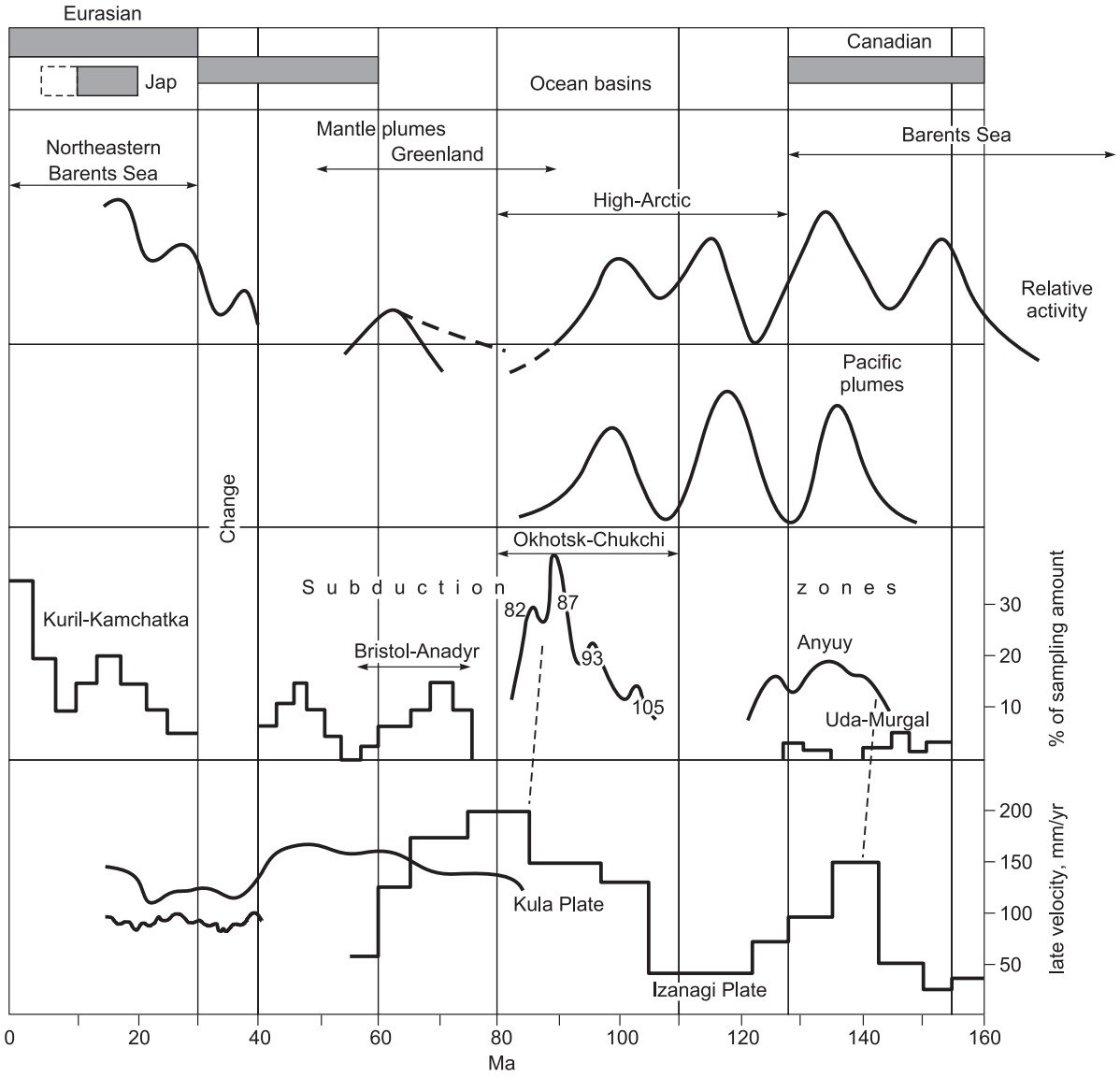

Fig. 10. Ages of Arctic oceanic basins, intensity of plume and subduction magmatism in the northwestern Pacific (Akinin et al., 2009; Dobretsov et al., 2008, 2013) correlated to Pacific plate velocity (Engebretson, et al., 2008; Akinin et al., 2009). Jap, Japan Sea basin. See text for explanations.

2.0% Na_2O and K_2O, i.e., its composition approached picritic alkali basalt or meimechite primary melt in the Maimecha-Kotui area of the Siberian trap province (Sobolev et al., 2009). Melt inclusions in olivine from meimechite contain on average 42% SiO_2, 7.5% Al_2O_3, 10% TiO_2, 13% FeO, 12% MgO, 13% CaO, 3% Na_2O, 2% K_2O, and 1.5% H_2O. In the calculated primary melt composition, MgO increases to 22%, while other oxides decrease to 38% SiO_2, 8% CaO, 4% Al_2O_3, 1.7% Na_2O, and 1.3% K_2O, with the alkalis notably lower than the Hawaii compositions. However, plume magma may be compositionally diverse in different place and time.

The orientation of the low-velocity zone in the asthenosphere at depths 100 and 300 km according to updated seismic tomography, with records of additional seismographs (Fig. 9), shows the northwestward motion of the Pacific plate (at an azimuth of 65°) and the motion of the plume in an N–S direction (Laske et al., 2009; Wolfe et al., 2009). The plate motion is better detectable in the 100 km depth section, the plume trace is clearer in the 300 km section, but the motions leave no record in the lower mantle (800 km section), at least in *P*-wave patterns: the isometrical anomaly looks like a spot ~300 km in diameter, with Δv_P ~0.5, Δv_S up to 1%, which corresponds to a plume of 100–120 km in diameter.

The Pacific plate had traveled about 6 000 km for 80 myr, at an average velocity of 7.5 cm/yr, slightly faster in the Emperor chain than in the Hawaii (7.7 cm/yr against 7.3 cm/yr), with minor variations about 46–20 Ma. The constant fast velocity of the large plate and the 60° bending of its path at ~46 Ma, as well as spreading deceleration in the East Pacific

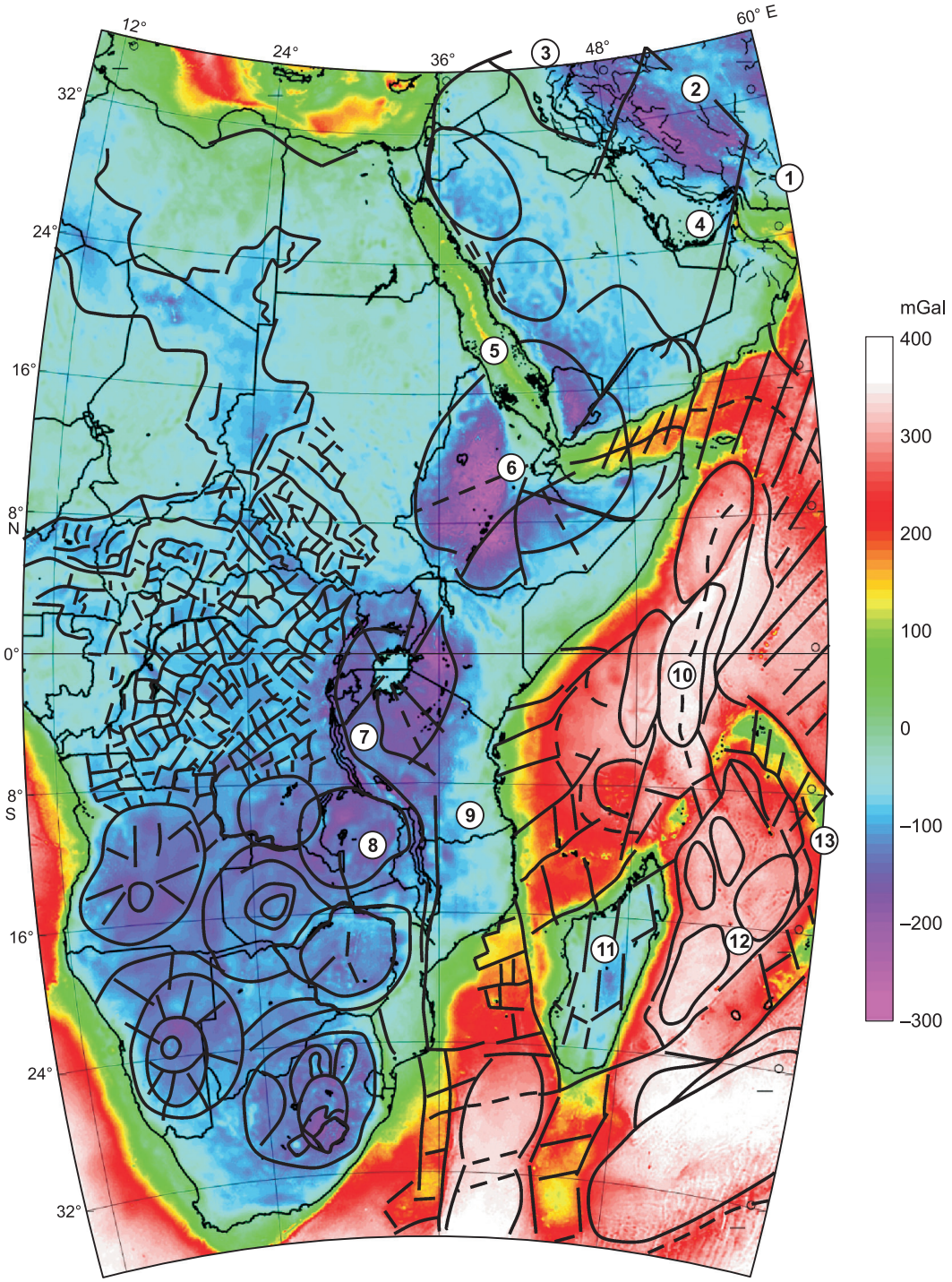

Fig. 11. Bouguer gravity anomalies in Africa and its surroundings. Mapped by A. Vasilevsky using the database of Andersen and Knudsen (2016). Dobretsov added structural lines in the Zagros zone (1, 2, 3), Persian Gulf (4), Red Sea (5), Afar mantle plume and triple junction (6), Tanzanian (7) and Zimbabwe (8) plumes, Somali plate (9), and South African group of Mesozoic plumes, oceanic structures near Somali and Madagascar (10, 11) and microcontinents of Seishelles (12) and Madagascar (13).

Rise (from 18 to 6 cm/yr) and in the Indian ocean (from 12 to 4 cm/yr), are worth special attention.

Over a time span of the past 150 Ma, the velocities of plates in the Pacific region varied depending on plume activity. The plate velocities and the related plumes in the Pacific and Arctic regions (Fig. 10) were compared previously (Dobretsov et al., 2013), with reference to (Akinin et al., 2009; Akinin, 2012). At 160–150 Ma, the Izanagi plate moved slowly at ~2 cm/yr, but accelerated to 15 cm/yr at ca. 140–135 Ma due to plume activity in the Central Pacific and Arc-

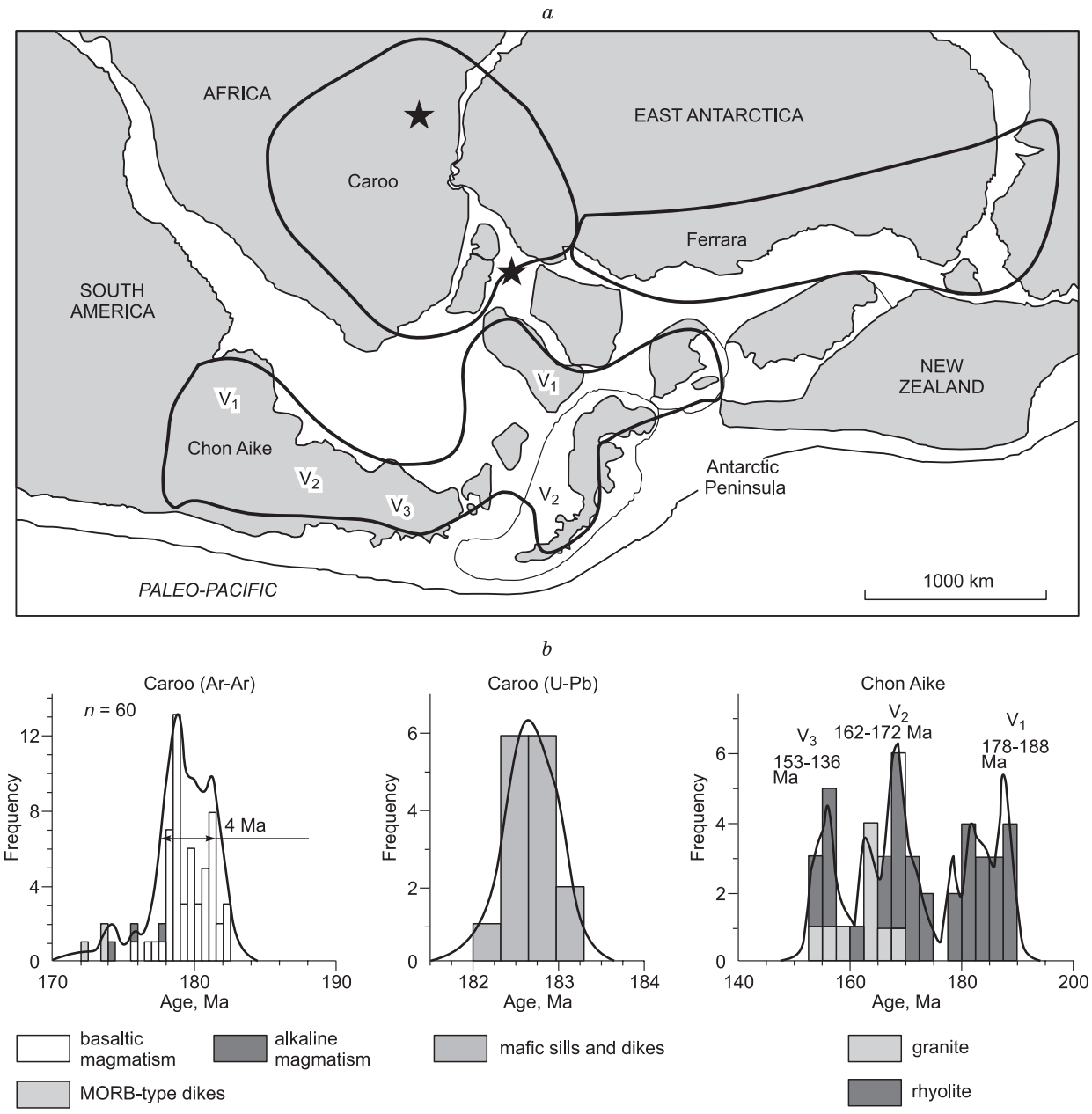

Fig. 12. A: Reconstruction of Gondwana in the Jurassic and flood basalts in the Caroo, Ferrara, and Chon Aike provinces, with stages V_1, V_2, and V_3 (Ben-Avraham et al., 1993; Brayn et al., 2002) (*a*); ages of Caroo and Chon Aike provinces (Lawver et al., 1985; McCarron and Larter, 1998; Pankhrust et al., 2000) (*b*).

tic regions, and possibly elsewhere. The plate acceleration was accompanied by subduction (Fig. 10) at 140 and 136 Ma, with peaks of related magmatism in the Uda-Murgal and Anyui island arcs. Than the plate slowed down when the plume activity declined, the subduction stopped, and the ensuing reduction of heat loss from the core increased its temperature. The core overheating induced another cycle of plume activity that peaked at 120 and then at 90 Ma, whereby the plate velocity increased to reach a maximum of 20 cm/yr for Kula by 85–80 Ma, and the subduction accelerated correspondingly, especially in the Okhotsk-Chukchi volcanic belt, where it peaked at 93, 87 and 82 Ma. The plume activity declined notably after 80 Ma, the plates again slowed down, and rapid subduction ceased. The peak of plume activity and the ensuing core cooling about 120–90 Ma ago led to a long period of stable geomagnetic polarity, heating of the asthenosphere, and increase in plate velocities to 20 cm/yr.

Note that the correlations of Fig. 10 are tentative and not yet global-scale; no models have been obtained for specific plume histories, asthenosphere heating, and plate acceleration. Some scenarios may be intermediate, with specific

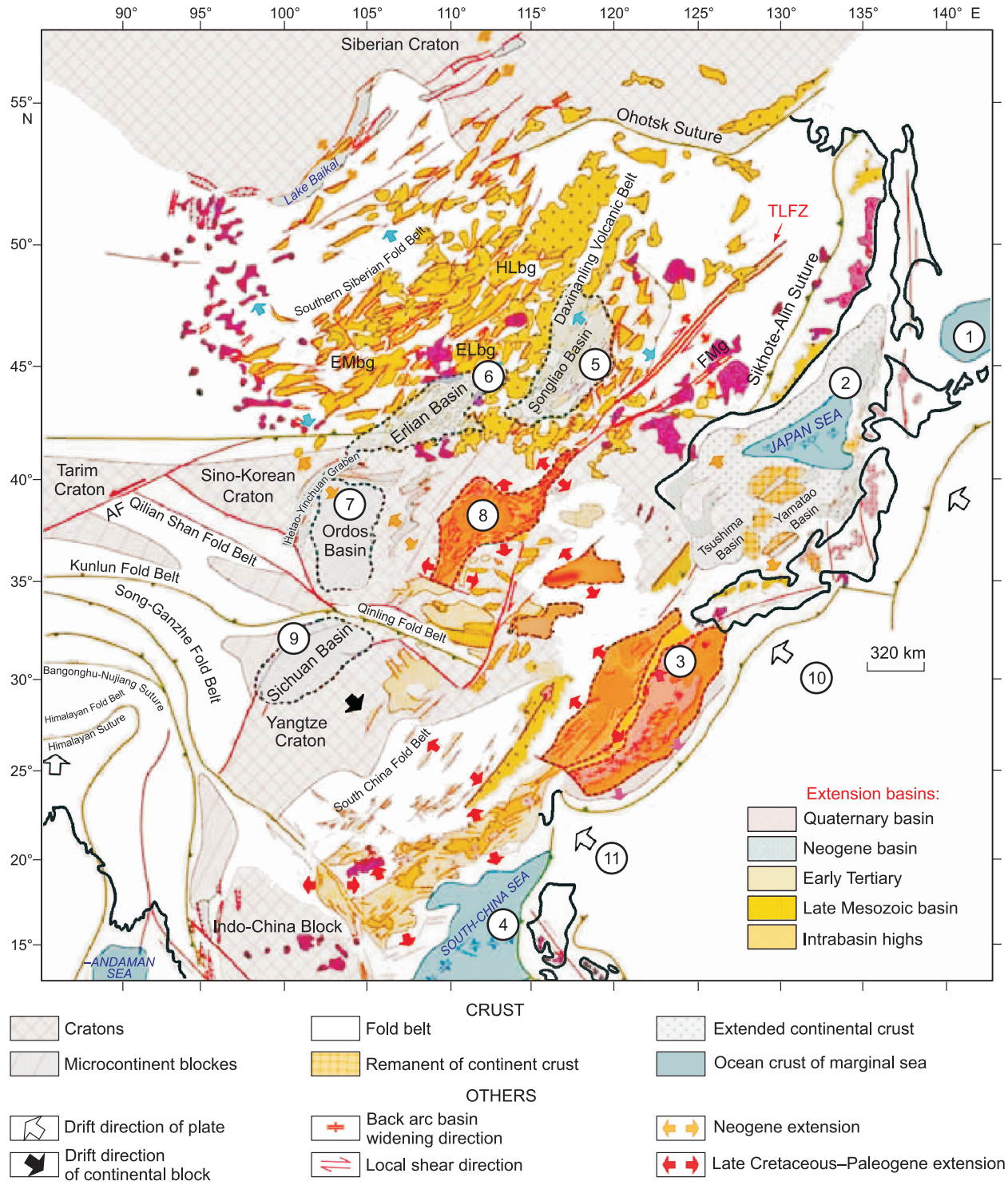

Fig. 13. Tectonic settings in East Asia (Russia, China, Korea, and Japan) and surrounding seas, modified after (Ren et al., 2002; Wang and Liang, 2019). TLFS, Tan Lu Fault System. Numbers 1–11 stand for major extension basins (see text), hatching and arrows show pull apart structures.

plumes accelerating some plates but decelerating the others. In any case, Figs. 4 and 10 demonstrate that the activity of plumes controls global tectonics by heating up the asthenosphere (and cooling down the core) and by affecting plate velocities and subduction rates. This interplay is responsible for the global periodicity of magmatism, with a cycle of ~30 Ma (Dobretsov et al., 2011; Dobretsov, 2013).

EFFECT OF PLUMES ON RIFTING AND CONTINENT BREAKUP

The East African mantle plumes provide a bright example of modern plume activity leading to breakup of continents. The chain of plumes in East Africa shows up in the Bouguer gravity pattern (Fig. 11) as lows of –100 to –300 mGal that stand out against the –100 to 0 mGal background.

The activity of the northernmost Afar plume induced alkali-basaltic magmatism since 55 Ma. The plume center corresponds to the Afar triple junction: the Gulf of Aden that has been opening for the past 30 myr; the Red Sea rift undergoing its latest evolution stage since 12 Ma; and the Afar rift that originated at 55 Ma and will likely remain a continental structure; the system also includes the Tajura rift at the junction of the Afar rift and the Aden Gulf, which has been active for the past 5 Ma. The Red Sea rift is flanked by 12–25 Ma rift-parallel dike belts, especially abundant in the northwestern part, and has the Suez and Dead Sea shear zones on its extension. The Dead Sea zone comprises a system of small magmatically active rift basins and may bridge the Red Sea rift with the southern Mediterranean in the future. This idea fits a probable scenario predicting that the Indian Ocean will open toward the Mediterranean and connect with the Atlantic, like the Paleozoic Paleotethys.

The Afar rift, together with the circular Tanzanian rift zone centered on Lake Victoria, and with the Zimbabwe rift (7 and 8, respectively, in Fig. 11) south of the Red Sea, make up the multi-stage East African system of Cenozoic rifts. The rift system separates Africa and the Somali plate (microcontinent), which is bordered in the east by three rift basins with oceanic crust and Jurassic-Cretaceous sediments separating it from the Madagascar and Seychelles continental blocks. Five other less prominent circular structures southwest of the Zimbabwe rift correspond to the Jurassic and Cretaceous Caroo and Etendeka plateaus that record the activity of Mesozoic plumes which induced Jurassic-Cretaceous rifting and the breakup of Gondwana, with separation of Africa from South America, Antarctica, and New Zealand.

The Jurassic pattern of Gondwanian continental blocks and the onset of South Atlantic opening are reconstructed in Fig. 12*a*, which shows the Caroo volcanic plateau, the Chon Aike and Ferrara volcanic belts, and the rifts (Ben-Avraham et al., 1993; Pankhurst et al., 2000; Bryan et al., 2002; Migdisova et al., 2017), and the plume centers (stars). Isotope dating of the Caroo and Chon Aike lavas (Fig. 12*b*) represents the propagation of volcanic activity from Caroo, which ended after a peak of plume magmatism about 180 Ma, to eruptions of mostly felsic lavas interacting with thick crust in the Chon Aike belt of South America (peak at ~150 Ma). Most of plume magmatic peaks since 150 Ma (Figs. 4 and 10) have been related to continent breakup. The mantle melting source at the modern Bouvet triple junction is heterogeneous due to mixing of MORB-type melts with a plume pyroxenite component mixed with old oceanic crust (Migdisova et al., 2017).

The ongoing continent breakup is the most active in South-East Asia and near the eastern Australian coast (Fig. 13). The Japan, Izu Bonin, and Mariana trenches sepa-

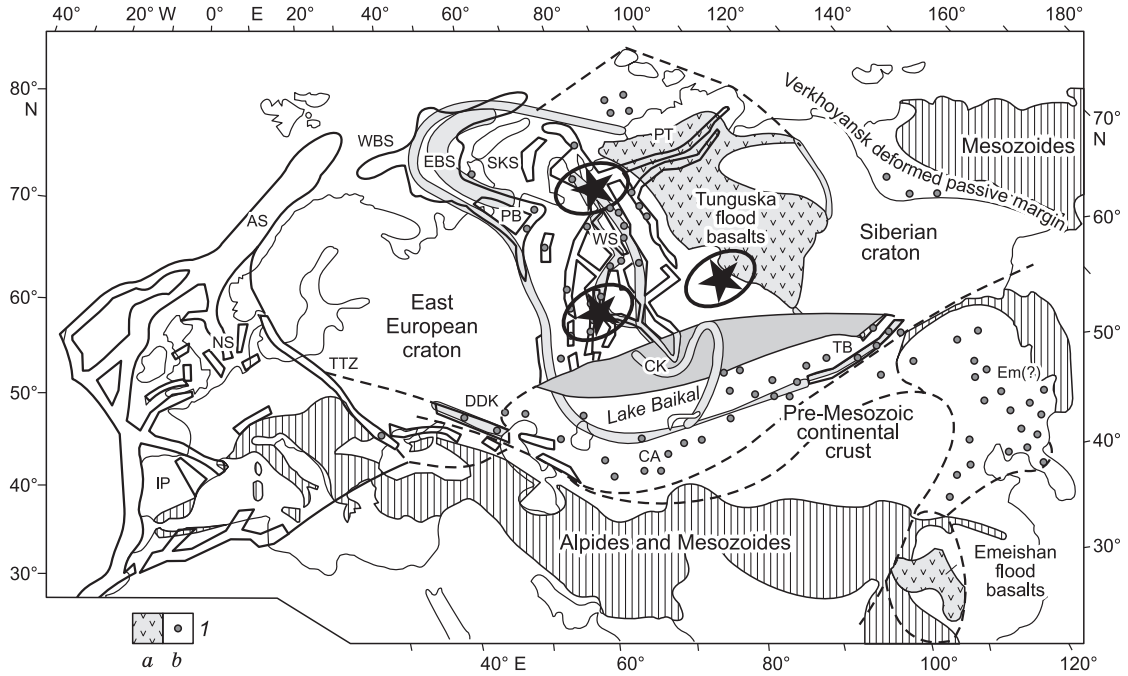

Fig. 14. Late Paleozoic large igneous provinces and rifts in Eurasia (Nikishin et al., 2002). Ovals with stars are plume centers in the Siberian Trap province. *1*, basalts as large fields (*a*) and separate outcrops and dikes (*b*).

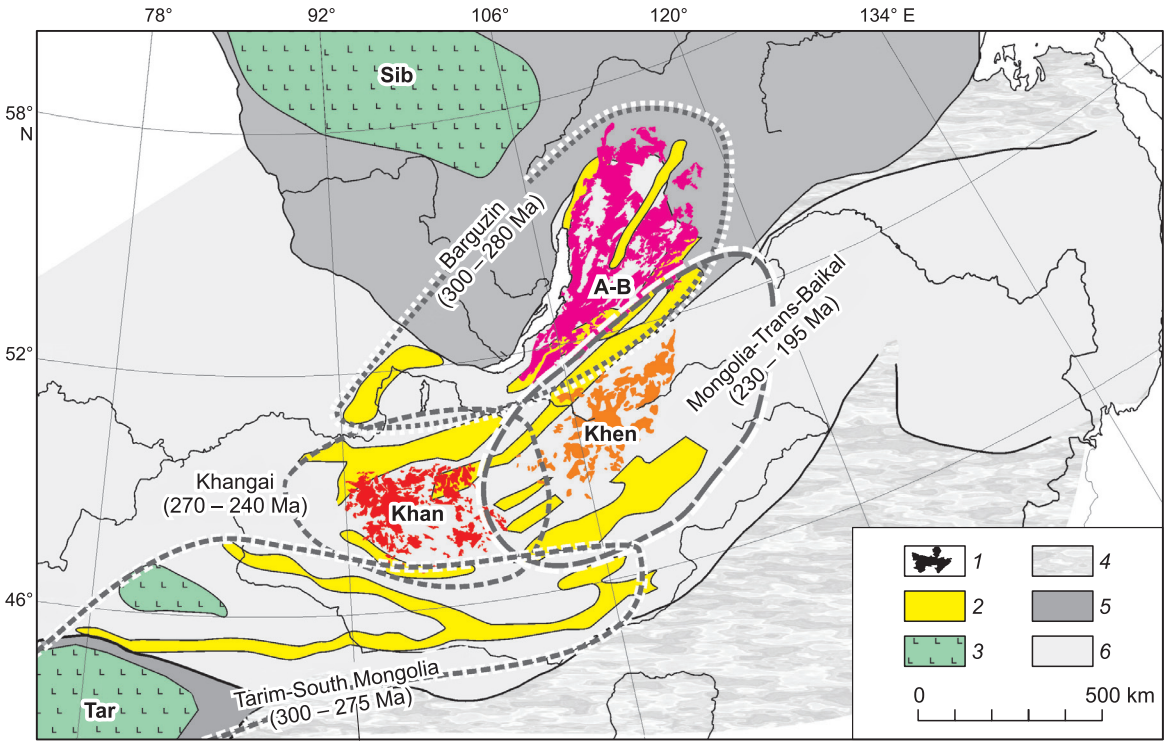

Fig. 15. Late Paleozoic-Triassic plutons and plume-related batholiths in Siberia and Mongolia (Yarmolyuk et al., 2013). *1*, granitic batholiths; *2*, zones of grabens and rift-related magmatism (alkali granite and bimodal volcanic series); *3*, Siberian craton and Tarim basin; *4*, oceanic basin complexes; *5*, cratons, *6,* orogens flanking cratons. Abbreviations stand for trap provinces (Sib = Siberia, Tar = Tarim) and batholith namess (A–V, Angara-Vitim; Khan, Khangai; Khen, Khentei).

rate the Pacific plate from island arcs of the respective names and their backarc basins of the Okhotsk (with the Kuril-Kamchatka trench), Japan, Philippine, East China, and South China seas. The Izu Bonin and Mariana arcs contain abundant boninites which are markers of early oceanic island arc settings (Crawford, 1989; Simonov et al., 1994).

The cratons and cratonic blocks of continental Asia (Siberia, Korea, Yangtze, Tarim, Indochina, and India) are

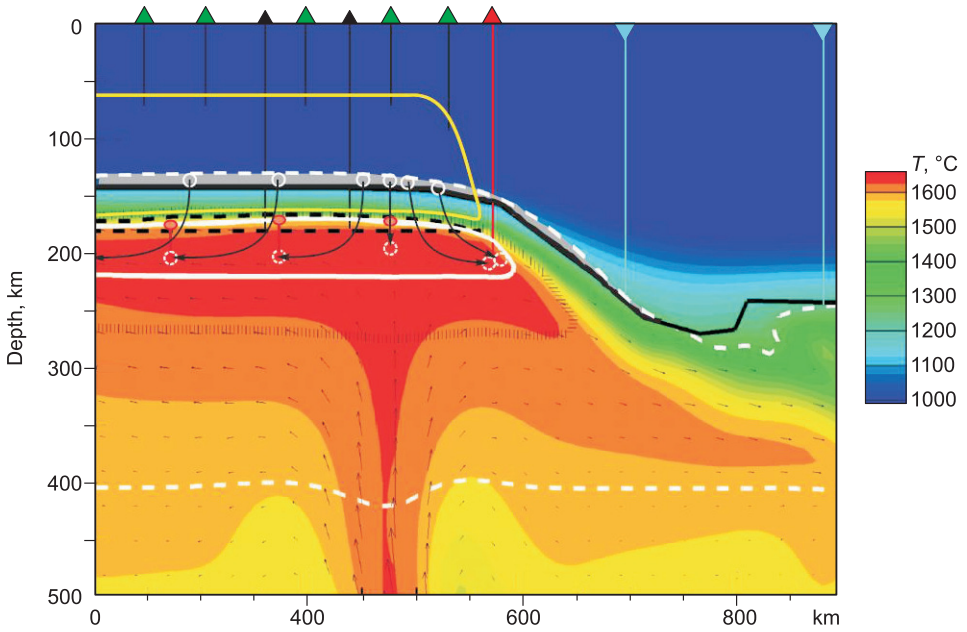

Fig. 16. Formation model of meimechite, Siberian traps, and kimberlites (Sobolev et al., 2009). See text for explanations.

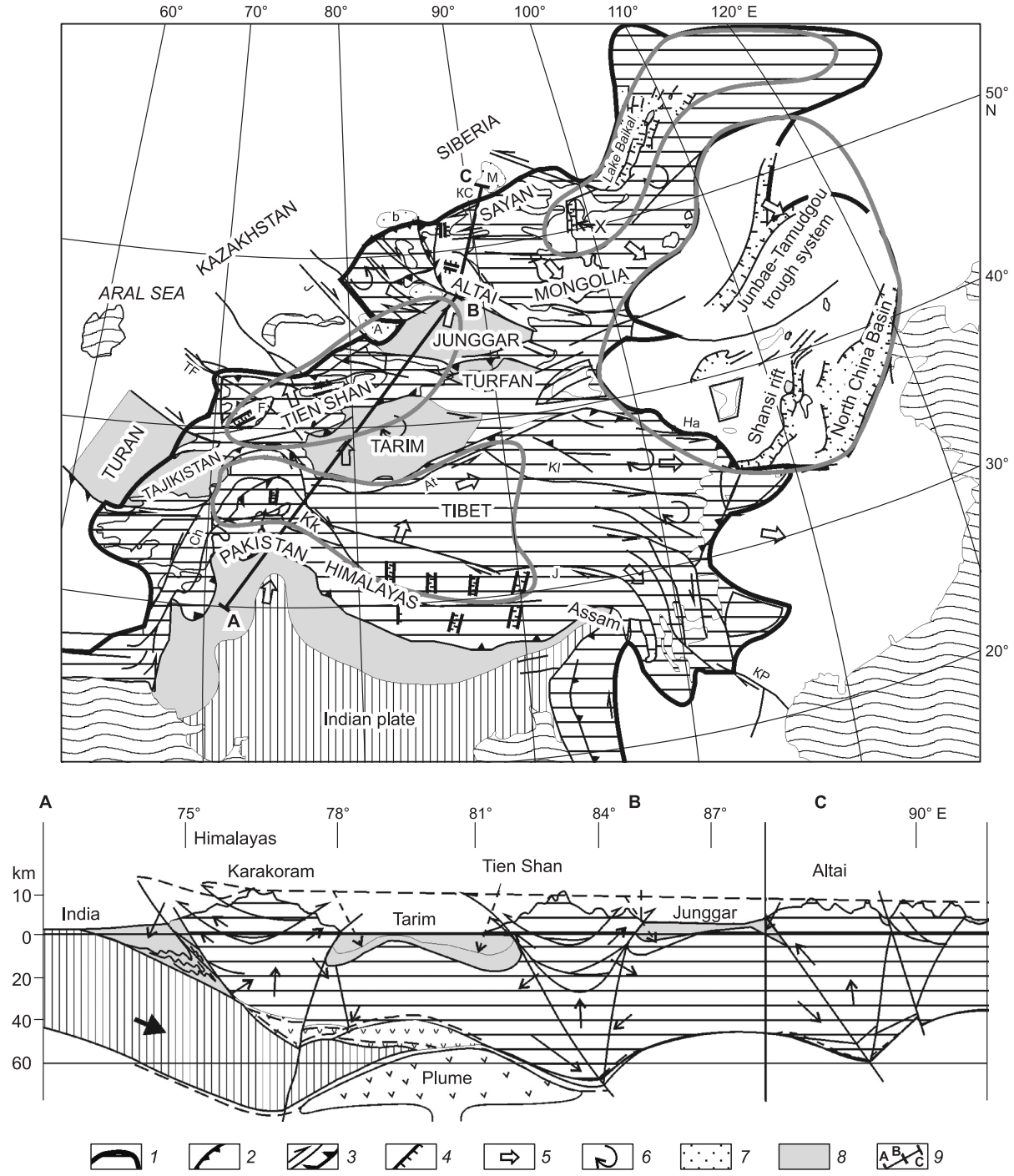

Fig. 17. Tectonic map and cross section from the Himalayas to the Altai (Dobretsov et al., 1996). *1*, contours of mantle plumes and uplifts; *2*, main thrusts; *3*, strike-slip and direction of motion; *4*, normal faults; *5*, motion of plates and blocks; *6*, modern rotation of blocks; *7*, Cenozoic basins (south to north), abbreviated as: F, Fergana; A, Ala-Kola; B, Barnaul; M, Minusa; KH, Khubargul; 8, large petroleum basins; 9, location of geological cross section. Large faults, abbreviated as: Ch, Chaman; Kk, Kara-Korum; At, Altyn-Tag, Kl = Kun-Lun; TF, Talas-Fergana; J, Junggar; Ha, Haysan.

separated by Paleozoic and Mesozoic orogenic belts. The zone between the Siberian and Indian cratons is affected by compression induced by the India-Eurasia collision (see below) whereas the remaining continents and the fringing seas are subject to extension with large rift-type or pull-apart basins. All backarc basins are of pull-apart type and have a mixed continental and newly generated oceanic crust: oceanic crust in the Kurile basin (1 in Fig. 13) and thin continental crust on its flanks; continental and oceanic crust in the northern periphery of the Japan Sea (2) and the Oka mi-

crocontinent blocks and thin crust in its southern part; thin continental and oceanic crust adjacent to the Ryukyu trench in the southeastern East China sea basin (3 in Fig. 13), which is deeper than the shallow northern part in the southeastern Sino-Korean craton (Wang and Liang, 2019). The chain of backarc basins (1–4) with combined thin continental and oceanic crust borders are associated with five rift basins on the continent (Fig. 13): Songliao (5), Erlian (6), Ordos (7), Chun-Lin (8), and Sichuan (9), which also locally have thin continental crust, e.g., a strip in the Erlian basin and north of it. The role of mantle plumes in the origin of the rifts remains open to discussions. The backarc basins (1–4) are commonly attributed to upwelling at the back of island arcs or to backarc spreading, as in the case of the Parece Vela basin in the Philippine Sea (10) or West Philippine basin (11), which are zones of parallel and oblique spreading, respectively. Other zones of oblique spreading may include the Japan Sea (2), the South Kurile basin (1) and the Commander basin near the Kamchatka shore (outside the area of Fig. 13). The models of pull-apart extension and rifting above a plume head were discussed previously by Polyansky and Dobretsov (2001) and Polyansky et al. (2018), respectively. However, basins 5–9 may have a plume origin, judging by their round shapes (especially 6–8) and the presence of the Daxinanling volcanic belt composed of bimodal alkali basalt and trachyrhyolite series on the periphery and on the extension of basins 5 and 6 (Wang and Liang, 2019). The breakup of Asia may lead to the formation of the Oka and Okusima microcontinents in Japan and in the Philippine Sea, as well as the Hainan, Thailand, and Shandong blocks in the northwest.

PLUMES BENEATH STABLE PLATES AND COMPRESSION ZONES

Plume magmatism in the late Paleozoic West European, Tarim, and Siberian trap continental provinces (Fig. 14) had no relation to the breakup of continents but was favorable for the formation of petroleum provinces (Nikishin et al., 2001).

The West European province includes rifts west and south of the East European craton, which surround the Iberian Peninsula and the Northern Sea (IP and NS, respectively, in Fig. 14) and extend northeast into the Arctic seas (AS in Fig. 14) and southeast along the Teisseyre-Tornquist zone and Dnieper-Donets rifts (TTZ and DDK, respectively, in Fig. 14). Alkali-basaltic and felsic lavas and granitic rocks in the province formed mainly in the 315–290 Ma interval, though some magmatic activity and mineralization continued till 270 Ma; some processes in the province were coeval to the Tarim magmatism and metallogeny (Nikishin et al., 2002; Dobretsov, 2008).

The Tarim province extends from the Caspian Sea as far as 120°E and partly overlaps with the Siberian trap province. It includes Central and Eastern Kazakhstan (CK, see Fig. 14), Central Asia with the Tien Shan and Tarim blocks (CA, Fig. 14), and Southeast Mongolia (TB, Fig. 14). The province consists of continental flood basalts (traps) and alkali basalts in the center and andesite, trachyandesite, trachyte, and trachyrhyolite elsewhere, especially in the Tien Shan and Kazakhstan regions (Borisenko et al., 2006; Dobretsov, 2008; Dobretsov et al., 2010). The southern border of the Tarim and West European provinces is truncated by the Neotethys structures. The ages of volcanics, granites, and mineralization in the Tarim province range from 300 to 275 Ma.

The Siberian trap province is located in the Siberian craton, in its southern and northern periphery and at the base of the West Siberian petroleum basin. The history of magmatism includes the early (265–255 Ma) and main (255–247 Ma) stages. The most abundant lithologies are basalts (Siberian traps) found as lavas, sills, and layered plutons with Cu–Ni–Pd mineralization in the Siberian craton; ultramafic (meimechite) lavas and alkali-ultramafic intrusions (Guli pluton) in the Maimecha-Kotui region; variable amounts of tuff and dike belts, with mineralization different from elsewhere in the province, in the southern craton part and in the Kuznetsk basin on its periphery; basalts, trachybasalts, as well as abundant rhyolite and less voluminous trachyandesite stripped in boreholes, in the basement of the West Siberian basin; 248 Ma basalts and rhyolites occur in the Semeitau area in the southern margin of the West Siberian basin. Thus, the Siberian trap province comprises several areas of magmatism: (1) Norilsk + Maimecha-Kotui centers, with volcanism and mineralization in the Khatanga Range, in the Taimyr Peninsula, and in the northern Siberian craton, including the periphery of the Anabar and Olenek uplifts; (2) northern West Siberia, junction of rifts (EBS and SKS) that may extend into the Barents Sea basin; (3) Angara center of magmatism and mineralization (possibly, in the Chadobets uplift) spreading to the southern Siberian craton and the Kuznetsk basin and its surroundings, as far as Northwestern Mongolia (plume centers are marked by stars in Fig. 14). In the Chadobets uplift, dolerite sills and basaltic tuffs coexist with exposed alkali-ultramafic rocks that formed during the early phase of magmatism constrained by 252 Ma or 265 Ma ages of early generation perovskite (Chebotarev et al., 2017).

Mineralization associated with the Tarim and Siberian plumes (Pirajno, 2000; Borisenko et al., 2006; Dobretsov et al., 2010; Izokh et al., 2016) includes unique Cu-Ni-Pd deposits in the Norilsk region and in West China; Cu-Mo porphyry deposits in Kuznetsk Alatau, Northern Mongolia, and Tien Shan; Fe and Fe–Ti–V deposits in the Angara area and Tien Shan; as well as diverse Au–Hg, Ag–Sb, and Sb–Hg deposits of small sizes but broad occurrence in the areas of all plumes.

The provinces of the Tarim and Siberian plumes, which also underwent collisional events, accommodate several large batholiths (Fig. 15): Barguzin batholith (300–280 Ma) coeval with the Tarim plume (300–270 Ma); Hangayn

batholith (270–240 Ma) coeval with the Siberian plume (265–240 Ma), and the Khentei batholith (230–195 Ma), with small occurrences of alkaline and ultramafic plume magmatism in its vicinities. The three batholiths in the southern periphery of the Siberian craton are associated with Siberian and Tarim trap magmatism and rift zones with alkaline granites and bimodal alkali volcanics (Yarmolyuk et al., 2013, 2019).

The settings of batholiths (Fig. 15) are generally consistent with the suggested model (Fig. 7) implying that granites can melt upon interaction of the plume margin with continental crust thickened during collisions, but have some particular features.

Of special interest is the origin of ultramafic lavas (meimechites) within the Siberian province, as well as possible relation between trap and kimberlite magmatism. The formation of Siberian traps and meimechites and their parentage to kimberlites was explained in a model (Fig. 16) suggested by Sobolev et al. (2009), which imaged a zone of melt stability (between isotherms of 1600 °C below and 1500 °C above) similar to that in the plume head from Fig. 7. Our models (Dobretsov et al., 2001, 2008) predict that melt accumulates in the plume head and fractionates in the chamber as a result of convection and cooling, with precipitation of crystals on the chamber bottom. The more sophisticated model of Sobolev et al. (2009) implies plume transport of carbonatite-bearing eclogite from an old subduction zone. Melting of eclogite at depths of 250–300 km produces carbonate–silicate melts which become canalized into porous magma guides (white circles and black arrows in Fig. 16). The eclogite-derived melts react with peridotite at depths about 170–150 km and form hybrid pyroxenite melt. The thin gray lens about 130 km is metasomatized lithosphere exposed to the effect of the pyroxenite melt. Yellow line bounds the lithospheric zone of delamination required for the formation of Siberian traps (Sobolev et al., 2009). Colored triangles on the surface in Fig. 16 mark different types of magmatism: black triangles are basalts erupted early during trap magmatism, related to melting of the pyroxenite source (Gudchikha Fm. picrite) and green triangles are basalts of the main phase formed by melting of the pyroxenite and peridotite sources (Sobolev et al., 2009). White dash line in Fig. 16 bounds the zone of meimechite melt stability at depths of 210–180 km, in the upper part of the eclogite melting zone. Red circles are primary meimechite melts that mixed with more voluminous pyroxenite magmas and failed to reach the surface, except for the margin of the meimechite lens where the gray pyroxenite shield pinches out (red triangle).

The model with pyroxenite magma generation from a plume source of an uncertain origin and old residual eclogite (Sobolev and Slutsky, 1984; Sobolev et al., 2009) appears too sophisticated, but the good idea of plume melts interacting with lithospheric peridotite (eclogite) is reasonable. The model of Fig. 7 (Dobretsov et al., 2001; Dobretsov, 2011) assumed cap collapse, with dissolution of the peridotite or eclogite blocks in plume melt as a main cause of mixing between mantle and lithospheric sources. The interaction of continental lithosphere and plumes in areas of trap magmatism was discussed in some publications (e.g., Lightfoot et al., 1993), but different approaches were suggested. Judging by Sr-Nd systematics of meimechites, they can come from asthenosphere while basalts may originate from fractionated melt of the plume head affected by metasomatized lithosphere (Izokh, pers. commun.).

In conclusion, it appears pertinent to discuss the role of mantle plumes in collisional compressive settings, for the case of the Cenozoic India–Eurasia collision and compression propagation from the Himalayas to Lake Baikal and the Stanovoy Range since 50 Ma. The map and the section across the Himalaya, Tarim, Tien Shan, Junggar, and Altai regions (Fig. 17) show that India together with the Himalaya foredeep are thrusting beneath the Himalayas and the Tibet, which compress the Tarim plate and make it thrusting beneath the Tien Shan. The latter, in its turn, presses upon the Junggar block inducing its thrusting under the Altai Mountains. Deformation in the Altai propagates to the East Sayan as far as the Siberian craton border and on northeastward to the Kodar-Udokan area. The ages of maximum uplift become successively younger from the Himalaya to the Altai: 25–10 Ma (Himalaya and Tibet), 15–10 Ma (Tien Shan), and 5–0 Ma (Altai and Baikal), as it was confirmed by apatite fission track thermochronology of mountain building events (De Grave et al., 2007, 2014; Buslov et al., 2008; Glorie et al., 2010, 2012; Buslov, 2012; Dobretsov et al., 2016).

The model of successive collisional orogenic events was first suggested by Molnar and Tapponnier (1975) and developed later by Dobretsov et al. (1996, 2001, 2016). The updated model assumed participation of mantle plumes in the process, with three plume provinces beneath Tibet and Pamir; Tien Shan and Junggaria; East Sayan and Baikal region (Fig. 17). Cenozoic plume magmatism in the Pamir, Tien Shan, East Sayan, and Baikal regions has been studied since 1950s, including in samples of spinel and garnet peridotite and eclogite xenoliths (Dobretsov et al., 1990, 1993, 1996).

Alkali-basaltic and ultrapotassic magmatism in Tibet, the key region in this respect (Chung et al., 2005; Lai et al., 2014; Wang et al., 2014; Guillot et al., 2019), forms a more than 2000 km long belt from 80° to 102°E. The rocks are a series of 50–38 Ma alkaline basalts from leucite and basanite tephrite to hawaite, mugearite, and benmoreite, and finally to trachyandesite with up to 12% ($K_2O + Na_2O$) and 8% K_2O. Younger (26–10 Ma) magmatism in Southern Tibet falls within a 1500 km belt and can be divided into two groups: (i) mugearite, benmoreite, trachyandesite, and trachyte which are similar to those from Northern Tibet but more potassic (8–15% $K_2O + Na_2O$), and (ii) adakite similar to subduction-related calc-alkaline rocks (up to 73% SiO_2), with signatures of lower crust melting (Gao et al., 2007). In Eastern Tibet, there are two main carbonatitic provinces as-

sociated with ultrapotassic kamafugites: 40–31 Ma Maoniuping in Sichuan (Xu et al., 2003) and 23–7 Ma Lixian in the western belt of Qiling (Xu et al., 2014). The occurrences of carbonatites are rare in compressive settings but are more common to rifting conditions and related to deep plume activity, such as Ol Doinyo Lengai in Tanzania or Kaiserstuhl in Germany (Guillot et al., 2019). Tibetan carbonatites are similar to those found in the Pleistocene magmatic province of the Apennines, which may result from interaction between asthenosphere and lithospheric mantle. The carbonatite and kamafugite associations at the borders of the Tibetan Plateau have been attributed to the activity of mantle plumes (Maruyama, 1994; Ernst and Buchan, 2002; Dobretsov et al., 2008). Meanwhile, as noted by Guillot et al. (2019, p. 964), "recent studies have re-evaluated Sichuan carbonatites as melting products from a lithospheric mantle intensely metasomatized by marine subducted sediments rather than originated from a mantle plume". This idea appears however doubtful, for several reasons: the 40–3 and 23– Ma ages of carbonatite and kamafugite contradicts their relation to subduction (which had stopped by that time); the low temperatures in lithospheric mantle (1070–1250 °C) inferred from xenolith data (Liu et al., 2011) are inconsistent with large-scale melting in lithospheric mantle; finally, synchronicity of plume magmatism in different Tibet, Tien Shan, Jonggaria, and Baikal settings makes thinking about some common mechanism that may drive block rotations and transfer of collisional compression 5000 km across the collisional front from the Indian plate as far as the Baikal region. Collisional compression hardly would propagate more than 1000 or 1500 km without plumes, as indictaed by the cases of Iran or the Caucasus, or old collisional zones.

The multi-stage compression and motions from the south and northeast are confirmed by seismic tomography (Guillot et al., 2019) which leads the authors to the conclusion that 40% of horizontal shortening are required north of the Indus suture zone during the India–Asia collision in order to accommodate the ~1000 km of Cenozoic convergence on the Asian side since 50 Ma. The present-day average elevation of 4800 m and 70 km crustal thickness, at homogeneous lithospheric thickening, may be due to intracontinental subduction along pre-existing sutures (Guillot et al., 2019). However, the seismic tomographic data for Southern Siberia (Zorin and Turutanov, 2005; Koulakov, 2008) are better consistent with plume effects.

The presence of mantle plumes detectable in seismic tomography images (Zorin and Turutanov, 2005; Koulakov, 2008) is further confirmed by gravity patterns of Southeastern Asia derived from satellite altimetry (Dobretsov et al., 2013; Dobretsov, 2008), with negative Bouguer anomalies in the zones of plumes and different patterns in zones of compression and extension (Fig. 18*a,b*). The Bouguer gravity field includes a prominent low (the strongest on Earth) beneath the Tibet and neighbor Qaidam uplifts (1 in Fig. 18*a*), an anomaly in Northern Mongolia and in the East Sayan in the north (2) coinciding with the field of Cenozoic volcanism and partly with the field of the Khangai batholith (Fig. 15*a*), and a small anomaly at Khentei (3) in the east, which likewise coincides with Cenozoic volcanics and the batholith (Fig. 15*a*). The northernmost fields (4) and (5) cover the northern Baikal region and the Vitim plateau and matches the Vitim field of Cenozoic volcanics and the Angara-Vitim batholith (Fig. 15). The zone of extension looks mute in the Bouguer gravity (Fig. 18*a*), but pull-apart structures similar to those of the Sea of Japan and its western surroundings appear as free-air gravity anomalies (Fig. 18*b*).

CONCLUSIONS

The interplay of plate and plume tectonics will remain a key issue of geodynamics for the next fifteen or twenty years, as many relevant aspects remain poorly understood. The discussions have focused on plumes younger than 300 Ma but did not consider Precambrian plumes. It is also unclear when plate and plume tectonics started to act to the full extent. These problems were partly discussed previously (Dobretsov, 2008, 2011; Kuzmin et al., 2018), but much controversy still remains. Namely, a special study is required for the role of plumes as main drivers of geological cycles, though research in this line began decades ago (Dobretsov et al., 1993; Kirdyashkin and Dobretsov, 2001; Grigoriev et al., 2009; Dobretsov, 2011). Other poorly resolved problems concern plume tectonics in terrestrial planets (Dobretsov, 2017) and plumes outside Eurasia, Africa, and the Northern Pacific.

This study has some innovative features: integration of seismic tomography of the lower mantle (Romanowicz and Gung, 2002; French and Romanowicz, 2015; Romanowicz et al., 2018) (Figs. 1, 2) and satellite altimetry data on the gravity field (Figs. 9, 18); correlation of plume head and plate velocity (Fig. 10); different proofs for the involvement of plumes in conjugate extension and compression zones (Figs. 14, 18); the idea that the plate velocity may depend on the number of plumes dissolved in the asthenosphere. The latter idea is relatively new, though there are other hypotheses.

This paper contributes to the Special Issue of *Russian Geology and Geophysics* devoted to the memory of Vladimir Stepanovich Sobolev, Full Member of the Russian Academy of Sciences, a prominent petrologist and mineralogist, my teacher. His paper on trap magmatism (Sobolev, 1936) was the first study of the Earth's largest LIP associated with mantle plumes, which has preserved its relevance till nowadays. The present study was inspired by the paper co-authored by A. and S. Sobolevs (Sobolev et al., 2009), two sons of Vladimir Sobolev. Vladimir Sobolev, together with his other son, Nikolay Sobolev, were among the first to formulate the idea that continental crust results from recycling of eclogitic oceanic crust in subduction zones unlike the oceanic crust production in mid-ocean ridges (Sobolev and Sobolev, 1975, 1977a,b). Another pioneering idea of V. Sobolev concerns involvement of of deep-seated hydro-

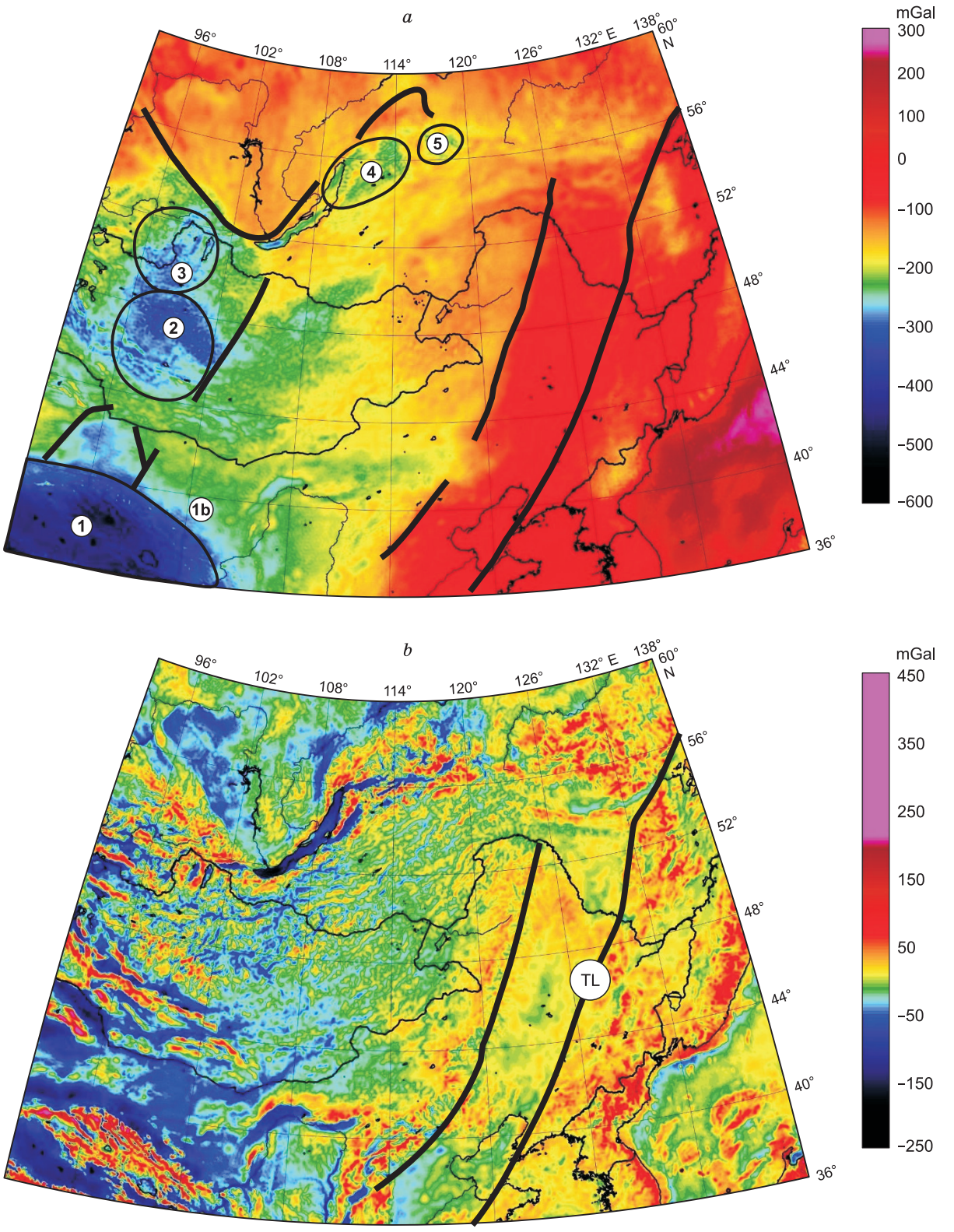

Fig. 18. Bouguer (*a*) and free-air (*b*) gravity anomalies in East Asia. *a*, Mantle plumes: Tibet (1), Khangai (2), Khovsgöl of East Sayan (3), Vitim (Burguzin) (4), Kodar-Udokan (5) (compare Figs. 15 and 17); *b*, Tan-Lu fault (TL) (Fig. 13).

carbons and CO_2 in diamond formation. The ideas by Vladimir Stepanovich have been a leading light in my life.

I wish to thank Nikolay Sobolev for collaboration and editorial efforts in preparing this volume. Thanks are extended to A. Sobolev for discussions, A. Vasilevsky for collaboration and advice on gravity field issues. E. Tsibizova and A. Lysov were helpful in the manuscript preparation. The paper profited from constructive criticism by A. Izokh.

The study was carried out as part of a Research Project run by the Institute of Petroleum Geology and Geophysics and was supported by grant 18-05-70109\18 Arctics from the Russian Federation for Basic Research.

REFERENCES

Abbot, D.M., Isley, A.E., 2002. The intensity, occurrence, and duration of superplume events and eras over geological time. J. Geodyn. 34, 265–307.

Akinin, V.V., 2012. Late Mesozoic and Cenozoic Magmatism in the Northern Circum-Pacific and Changes in the Lower Crust [in Russian]. Author's Abstract, Doctor Thesis. IGEM, Moscow.

Akinin, V.V., Miller, E.L., Wooden, J.L., 2009. Petrology and geochronology of crustal xenoliths from the Bering Strait region: Linking deep and shallow processes in extending continental crust, in: Crustal Cross Sections from the Western North American Cordillera and Elsewhere: Implications for Tectonic and Petrologic Processes. Geol. Soc. Am. Spec. Paper 456, pp. 39–68.

Andersen, O.B., Knudsen, P., 2016. Deriving the DTU15 Global high resolution marine gravity field from satellite altimetry, in: ESA Living Planet Symposium. Prague. Paper 1558.

Artyushkov, E.V., 1993. Physical Tectonics [in Russian]. Nauka, Moscow.

Behr, W., 2019. Earth's evolution explored. Nature 570, 38–39.

Behr, W.M., Becker, T.W., 2018. Sediment control on subduction plate speeds. Earth Planet. Sci. Lett. 502, 166–173.

Ben-Avraham, Z., Hartnady, C.J.H., Malan, J.A., 1993. Early tectonic extension between the Agulhas Bank and the Falkland Plateau due to the rotation of the Lafonia microplate. Earth Planet. Sci. Lett. 117, 43–58.

Bercovici, D., 2003. The generation of plate tectonics from mantle convection. Earth Planet. Sci. Lett. 205, 107–121.

Bogdanov, N.A., Dobretsov, N.L., 2002. The Okhotsk volcanic oceanic plateau. Geologiya i Geofizika (Russian Geology and Geophysics) 43(2), 100–114 (87–99).

Borisenko, A.S., Sotnikov, V.I., Izokh, A.E., Polyakov, G.V., Obolensky, A.A., 2006. Permo-Triassic mineralization in Asia and its relation to plume magmatism. Russian Geology and Geophysics (Geologiya i Geofizika) 47 (1), 166–182 (170–186).

Bryan, S.E., Riley, T.R., Jerram, D.A., Stephens, C.J., Leat, P.T., 2002. Silicic volcanism: An undervalued component of large igneous provinces and volcanic rifted margins, in: Menzies, M.A., Klemperer, S.L., Ebinger, C.J., Baker, J. (Eds.), Volcanic Rifted Margins. Boulder, Colorado, Geol. Soc. Am. Spec. Paper 362, pp. 99–120.

Buslov, M.M., 2012. Geodynamic nature of the Baikal rift zone and its sedimentary filling in the Cretaceous-Cenozoic: the effect of the far-range impact of the Mongolo-Okhotsk and Indo-Eurasian collision. Russian Geology and Geophysics (Geologiya i Geofizika) 53 (9), 955–962 (1245–1255).

Buslov, M.M., Kokh, D.A., De Grave, J., 2008. Mesozoic-Cenozoic tectonics and geodynamics of the Altai, Tien-Shan, and Northern Kazakhstan, from apatite fission-track data. Russian Geology and Geophysics (Geologiya i Geofizika) 49 (9), 648–654 (862–870).

Chebotarev, D.A., Doroshkevich, A.G., Sharygin, V.V., Yudin, D.S., Ponomarchuk, A.V., Sergeev, S.A., 2017. Geochronology of the Chuktukon carbonatite massif, Chadobets uplift (Krasnoyarsk territory). Russian Geology and Geophysics (Geologiya i Geofizika) 58 (10), 1222–1231 (1542–1553).

Chung, S.L., Chu, M.F., Zhang, Y., Xie, Y., Lo, C.H., Lee, T.Y., Lan, C.Y., Li, X., Zhang, Q., Wang, Y., 2005. Tibetan tectonic evolution inferred from spatial and temporal variations in post-collisional magmatism. Earth Sci. Rev. 68 (3–4), 173–196.

Coffin, M., Eldholm, O., 1994. Large igneous provinces: crustal structure, dimensions, and external consequences. Rev. Geophys. 32, 1–36.

Coleman, R.G., 1977. Ophiolites. Springer-Verlag, New York.

Condie, K., 2004. Supercontinents and superplume events: distinguishing signals in the geologic record. Phys. Earth Planet. Inter. 146, 319–332.

Courtillot, V., Davaille, A., Besse, J., Stock, J., 2003. Three distinct types of hotspots in the Earth's mantle. Earth Planet. Sci. Lett. 205, 295–308.

Cox, A., Hart R.B., 1986. Plate Tectonics: How it Works. Blackwell Scientific Publications, Palo Alto, California.

Crawford, A.F. (Ed.), 1989. Boninites. Unwyn-Hyman, London.

De Grave, J., Buslov, M.M., Van den Haute, P., 2007. Distant effects of India–Eurasia convergence and Mesozoic intracontinental deformation in Central Asia: constraints from apatite fission-track thermochronology. J. Asian Earth Sci. 29 (2–3), 188–204.

De Grave, J., De Pelsmaeker, E., Zhimulev, F.I., Glorie, S., Buslov, M.M., Van den Haute, P., 2014. Meso-Cenozoic building of the northern Central Asian Orogenic Belt: thermotectonic history of the Tuva region. Tectonophysics 621, 44–59.

Dobretsov, N.L., 1980. Introduction into Global Petrology [in Russian]. Nauka, Novosibirsk.

Dobretsov, N.L., 2005. 250 Ma large igneous provinces of Asia: Siberian and Emeishan traps (plateau basalts) and associated granitoids. Russian Geology and Geophysics (Geologiya i Geofizika) 46 (9), 847–868 (870–890).

Dobretsov, N.L., 2008. Geological implications of the thermochemical plume model. Russian Geology and Geophysics (Geologiya i Geofizika) 49 (7), 441–454 (587–604).

Dobretsov, N.L., 2010. Global geodynamic evolution of the Earth and global geodynamic models. Russian Geology and Geophysics (Geologiya i Geofizika) 51 (6), 592–610 (761–784).

Dobretsov, N.L., 2011. Fundamentals of Tectonics and Geodynamics [in Russian]. NSU, Novosibirsk.

Dobretsov, N.L., 2017. The evolution of planets. Venus as the Earth's probable future. Russian Geology and Geophysics (Geologiya i Geofizika) 58 (1), 1–11 (3–16).

Dobretsov, N.L., Kirdyashkin, A.G., 1994. Mantle Geodynamics [in Russian]. Izd. SO RAN, Novosibirsk.

Dobretsov, N.L., Litasov, K.D., Sobolev A.V., 1990. Evidence of reaction melt percolation in the upper mantle, according to data on mantle xenoliths from basalts of the Vitim and Udokan volcanic fields in Transbaikalia. Doklady AN SSSR 368 (4), 525–529.

Dobretsov, N.L., Kirdyashkin, A.G., Gladkov I.N., 1993. Problems of deep geodynamics and modeling of mantle plumes. Geologiya i Geofizika (Russian Geology and Geophysics) 34 (12), 3–20 (5–24).

Dobretsov, N.L., Buslov, M.M., Delvaux, D., Berzin, N.A., Ermikov, V.D., 1996. Meso- and Cenozoic tectonics of the central mountain belt: effects of lithospheric plate interaction and mantle plumes. Intern. Geol. Rev. 38, 430–466.

Dobretsov, N.L., Kirdyashkin, A.G., Kirdyashkin, A.A., 2001. Deep-Seated Geodynamics [in Russian]. Geo, Novosibirsk.

Dobretsov, N.L., Kirdyashkin, A.A., Kirdyashkin, A.G., Vernikovsky, V.A., Gladkov I.N., 2008. Modelling of thermochemical plumes and implications for the origin of the Siberian traps. Lithos 100 (1), 66–92.

Dobretsov, N.L., Borisenko, A.S., Izokh, A.E., Zhmodik, S.M., 2010. A thermochemical model of Eurasian Permo-Triassic mantle plumes as a basis for prediction and exploration for Cu–Ni–PGE and rare-metal ore deposits. Russian Geology and Geophysics (Geologiya i Geofizika) 51 (9), 903–924 (1159–1187).

Dobretsov, N.L., Vernikovsky, V.A., Simonov, V.A., Karyakin, Y.V., Korago, E.A., 2013. Mesozoic-Cenozoic volcanism and geodynamic events in the central and eastern Arctic. Russian Geology and Geophysics (Geologiya i Geofizika) 54 (8), 874–887 (1126–1144).

Dobretsov, N.L., Vasilevsky, A.N., Nevedrova, N.N., Buslov, M.M., Vetrov, E.V., 2016. Cenozoic history of topography in southeastern Gorny Altai: thermochronology and resistivity and gravity records. Russian Geology and Geophysics (Geologiya i Geofizika) 57 (11), 1525–1534 (1937–1948).

Engebretson, D.C., Cox, A., Gordon, R.G., 2008. Relative motions between oceanic plates in the Pacific basin. J. Geophys. Res. 36 (5), 431–432.

Ernst, R.E., 2014. Large Igneous Provinces. Cambridge University Press.

Ernst, R.E., Buchan, K.L., 2002. Maximum size and distribution in time and space of mantle plumes: evidence from large igneous provinces. J. Geodyn. 34 (2), 309–342.

French, S.W., Romanowicz, B., 2015. Broad plumes rooted at the base of the Earth's mantle beneath major hotspots. Nature 525, 95–99.

Gao, Y., Hou, Z., Kamber, B.S., Wei, R., Meng, X., Zhao, R., 2007. Adalite-like porphyries from the south Tibetan collisional zones: evidence for slab melt metasomatism. Contrib. Mineral. Petrol. 153 (1), 105–120.

Glorie, S., De Grave, J., Buslov, M.M., Elburg, M.A., Stockli, D.F., Gerdes, A., van den Haute, P., 2010. Multi-method chronometric constraints on the evolution of the Northern Kyrgyz Tien Shan granitoids (Central Asian Orogenic Belt): from emplacement to exhumation. J. Asian Earth Sci. 38, 131–146.

Glorie, S., De Grave, J., Buslov, M.M., Zhimulev, F.I., Elburg, M.A., Van den Haute, P., 2012. Structural control on Meso-Cenozoic tectonic reactivation and denudation in the Siberian Altai: insights from multi-method thermochronometry. Tectonophysics 544–545, 75–92.

Graham, I.J., Gulson, B.L., Mizon, L., 1992. Petrogenesis of Late Cenozoic volcanic rocks from the Tanpo Volcanic zone, New Zeland in the light of new isotopic data. Geochim. Cosmochim. Acta 56, 2797–2819.

Grigoriev, A.I., Dobretsov, N.L., Zavarzin, G.A., Rozanov, A.Yu., Spirin A.S. (Eds.), 2009. Problems of Life Origin [in Russian]. PIN RAS, Moscow.

Guillot, S., Goussin, F., Airaghi, L., Replumaz, A., De Sigoyer, J., Cordier, C., 2019. How and when did the Tibetan plateau grow? Russian Geology and Geophysics (Geologiya i Geofizika) 60 (9), 957–977 (1207–1230).

Hanski, E., Walker, R.J., Huhma, H., Polyakov, G.V., Balykin, P.A., Hoa, T.T., Phuong, N.T., 2004. Origin of the Permian — Triassic komatiitees, northwestern Vietnam. Contrib. Mineral. Petrol. 147, 453–469.

Hoa, T.T., Anh, T.T., Phuong, N.T., Van, V.V., Nien, B.A., Izokh, A.E., Polyakov, G.V., Borisenko, A.S., Balykin, P.A., Rudnev, S.N., 2008. Permo-Triassic magmatism and metallogeny of northern Vietnam in relation to the Emeishan plume. Russian Geology and Geophysics (Geologiya i Geofizika) 49 (7), 480–491 (637–651).

Izokh, A.E., Fedoseev, G.S., Polyakov, G.V., Nikolaeva, I.V., Palesskii, S.V., Medvedev, A., 2016. Distribution of PGE in Permo-Triassic basalts of the Siberian large igneous province. Russian Geology and Geophysics (Geologiya i Geofizika) 57 (5), 809–821 (1028–1042).

Kirdyashkin, A.G., Dobretsov, N.L., 1991. Modeling of mantle convection in the double layer. Doklady RAN 318 (4), 946–949.

Kirdyashkin, A.G., Dobretsov, N.L., 2001. Structure of mantle convection and plumes: Effect on periodicity of magmatism, in: Global Change [in Russian]. Izd. SO RAN, Novosibirsk, pp. 27–41.

Kirdyashkin, A.G., Kirdyashkin, A.A., Dolgov V.Yu., 1994. Experimental modeling of unsteady-state convective flows in the lower mantle of the earth. Dokl. Akad. Nauk 338 (3), 394–396.

Kirdyashkin, A.G., Dobretsov, N.L., Kirdyashkin, A.A., 2000. Turbulent convection and magnetic field of the outer Earth's core. Geologiya i Geofizika (Russian Geology and Geophysics) 41 (5), 579–592 (601–612).

Koulakov, I.Yu., 2008. Upper mantle structure beneath Southern Siberia and Mongolia, from regional seismic tomography. Russian Geology and Geophysics (Geologiya i Geofizika) 49 (3), 187–196 (248–261).

Kurz, M.D., Geist, D., 1999. Dynamics of the Galapagos hotspot from helium isotope geochemistry. Geochim. Cosmochimica Acta 63 (23–24), 4139–4156.

Kuzmin, M.I., Goryachev, N.A., Yarmolyuk, V.V., Kotov, A.B., 2018. Magmatism and metallogeny of the early Earth as a reflection of its geologic evolution. Russian Geology and Geophysics (Geologiya i Geofizika) 59 (12), 1535–1547 (1924–1940).

Lai, S.C., Qin, J.F., Khan, J., 2014. The carbonated source region of Cenozoic mafic and ultramafic lavas from West Cinling. Gondwana Res. 2547, 1501–1516.

Larson, R.L., Olson, P., 1991. Mantle plume control magnetic reversal frequency. Earth Planet. Sci. Lett. 107, 437–447.

Laske, G., Collins, J.A., Wolfe, C.J., Solomon, S.C., Detrick, R.S., Orcutt, J.A., Bercovici, D., Hauri, E.H., 2009. Probing the Hawaiian hot spot with new ocean bottom instruments. EOS Transactions, AGU 90, 362–363.

Lawver, L., Sclater, J., Meinke, L., 1985. Mesozoic and Cenozoic reconstructions of the South Atlantic. J. South Am. Earth Sci. 114, 233–254.

Le Pichon, X., 1968. Sea floor spreading and continental drift. J. Geophys. Res. 73, 3661–3697.

Le Pichon, X., Francheteau J., Bonnin J., 1997. Plate Tectonics. Elsevier, Amsterdam.

Lightfoot, P.C., Hawkesworth, C.J., Hergt, J., Naldrett, A.J., Gorbachev, N.S., Fedorenko, V.A., Doherty, W., 1993. Remobilisation of the continental lithosphere by a mantle plume: major-, trace-element, and Sr-, Nd-, and Pb-isotope evidence from picritic and tholeiitic lavas of the Noril'sk District, Siberian Trap, Russia. Contrib. Mineral. Petrol. 114, 171–188.

Litasov, K.D., Shatsky A.F., 2016. Core Structure and Composition [in Russian]. Izd. SO RAN, Novosibirsk.

Liu, C.Z., Wu, F.Y., Chung, S.L., Zhao, Z.D., 2011. Fragments of hot and metasomatized mantle lithosphere in Middle Miocene ultrapotassic lavas, southern Tibet. Geology 39, 923–926.

Maruyama, Sh., 1994. Plume tectonics. J. Geol. Soc. Japan 100, 24–49.

Mazaud, A., Laj, C., 1991. The 15 m.y. geomagnetic reversal periodicity: guantitative test. Earth Planet. Sci. Lett. 107, 689–696.

McCarron, J.J., Larter, R.D., 1998. Late Cretaceous to early Tertiary subduction history of the Antarctic Peninsula. J. Geol. Soc. London 155, 255–268.

Migdisova, N.A., Sobolev, A.V., Sushevskaya, N.M., Dubinin, E.P., Kuzmin, D.V., 2017. Mantle heterogeneity at the Bouvet triple junction based on the composition of olivine phenocrysts. Russian Geology and Geophysics (Geologiya i Geofizika) 58 (11), 1289–1304 (1633–1648).

Molnar, P. Tapponnier, P., 1975. Cenozoic tectonics of Asia. Effects of a continental collision. Science 189, 419–426.

Morgan, W.J., 1971. Convection plumes in the lower mantle. Nature 230 (5288), 42–43.

Nikishin, A.M., Ziegler, P.A., Abbot, D., Brunet, M.-F., Cloetingh, S., 2002. Permo-Triassic intraplate magmatism and rifting in Eurasia:

Implications for mantle plumes and mantle dynamics. Tectonophysics 351, 3–39.

Pankhurst, R.J., Riley, T.R., Fanning, C.M., Kelley, S.R., 2000. Episodic silicic volcanism along the proto-Pacific margin of Patagonia and the Antarctic Peninsula: Plume and subduction influences associated with the break-up of Gondwana. J. Petrol. 41, 605–625.

Pirajno, F., 2000. Ore deposits and mantle plumes. Kluwer Acad. Publ., Amsterdam.

Polyansky, O.P., Dobretsov, N.L., 2001. Model of the development of a sedimentary basin of the pull-apart type. Dokl. Earth Sci. 380 (7), 800–805.

Polyansky, O.P., Reverdatto, V.V., Babichev, A.V., Sverdlova, V.G., Prokopiev, A.V., Koroleva, O.V., Tomshin, M.D., Vasiliev, D.A., 2018. The nature of the heat source of mafic magmatism during the formation of the Vilyui Rift based on the ages of dike swarms and results of numerical modeling. Russian Geology and Geophysics (Geologiya i Geofizika) 59 (10), 1217–1236 (1519–1541).

Ren, J., Tamaki, K., Li, S., Junxia, Z., 2002. Late Mesozoic and Cenozoic rifting and its dynamic setting in Eastern China and adjacent areas. Tectonophysics 344 (3–4), 175–205.

Romanowicz, B., Gung, Y.S., 2002. Superplumes from the core-mantle boundary to the lithosphere: Implications for heat flux. Science 296 (5567), 513–516.

Romanowicz, B., Ceo, A., Godwal, B., Wenk, R., Ventosa, S., Jeanloz, R., 2018. Seismic anisotropy in the Earth's innermost inner core: Testing structural models against mineral physics predictions. Geophys. Res. Lett. 43 (1), 93–100.

Schilling, J.G. Kingsley, R., Fontignie, D., Poreda, R., Xue, S., 1999. Dispersion of the Jan Mayen and Iceland mantle plumes in the Arctic: A He-Pb-Nd-Sr isotope tracer study of basalts from the Kolbeinsey, Mohns, and Knipovich Ridges. J. Geophys. Res. 104 (B5), 10543–10569.

Shellnutt, J.G., 2014. The Emeishan large igneous province: a synthesis. Geosci. Front. 5, 369–394.

Simonov, V.A., Dobretsov, N.L., Buslov, M.M., 1994. Boninite series in structures of the Paleoasian ocean. Russian Geology and Geophysics (Geologiya i Geofizika) 35 (7–8), 157–171 (182–199).

Sobolev, A.V., Slutsky, A.B., 1984. Composition and crystallization conditions of the primary meimechite melt of Siberia in the context of the general problem of ultramafic magma. Soviet Geology and Geophysics (Geologiya i Geofizika) 25 (12), 97–110.

Sobolev, A.V., Hofmann, A., Sobolev, S., Nikogosian, I., 2005. An olivine-free mantle source of Hawaiian Shield basalts. Nature 434, 590–597.

Sobolev, A.V., Kuzmin, D.V., Sobolev, S.V., Petrunin, A.G., Malitch, K.N., 2009. Siberian meimechites: origin and relation to flood basalts and kimberlites. Russian Geology and Geophysics (Geologiya i Geofizika) 50 (12), 999–1033 (1293–1334).

Sobolev, A.V., Hotman, A.W., Kuzmin, D.V., Yaxley, G.M., Arndt, N.T., Chung, S.L., Danyushevsky, L.V., Elliott, T., Frey, F.A., Garcia, M.O., Gurenko, A.A., Kamenetsky, V.S., Kerr, A.C., Krivolutskaya, N.A., Matvienkov, V.V., Nikogosian, I.K., Rocholl, A., Sigurdsson, I.A., Sushchevskaya, N.M., Teklay, M., 2007. The amount of recycled crust sources of mantle derived melts. Science 316 (5825), 412–417.

Sobolev, N.V., 1974. Mantle Xenoliths in Kimberlites and the Upper Mantle Composition [in Russian]. Nauka, Novosibirsk.

Sobolev, S.V., Brown, M., 2019. Role of major erosion events in Earth's dynamics. Nature 570, 52–57.

Sobolev, V.S., 1936. Petrology of continental flood basalts in the Siberian craton (Siberian Traps). Glavsevmorput, Leningrad. Transactions, Arctic Institute, Issue 18.

Sobolev, V.S., Sobolev, N.V., 1975. The problem of crust growth. Dokl. AN SSSR 221 (2), 435–438.

Sobolev, V.S., Sobolev A.V., 1977a. The composition of deep pyroxenes and problems of eclogite barrier. Soviet Geology and Geophysics (Geologiya i Geofizika) 18 (12), 46–59.

Sobolev, V.S., Sobolev A.V., 1977b. An eclogite barrier in re-crystallization of natural basalt under high pressure. Dokl. Akad. Nauk SSSR 234 (4), 896–899.

Sorokhtin, O.G., 1974. Global Evolution of the Earth. Nauka, Moscow.

Torsvik, T.H., Cocks, L.R., 2017. Earth History and Paleogeography. Cambridge University Press.

Wang, C., Bai, J., Zhao, X., Li, Y., Graham, S.A., He, D., Ran, B., Meng, J., 2014. Outward growth of the Tibetan Plateau during the Cenozoic: A review. Tectonophysics 621, 1–43.

Wang, H., Liang, J., 2019. Tectonic evolution of late Mesozoic-Cenozoic basins in eastern China and implications for Pacific Plate subduction. Russian Geology and Geophysics (Geologiya i Geofizika) 60 (4), 472–491 (555–577).

Wilson, J., 1965. Evidence from ocean islands suggesting movement in the earth. Philos. Trans., R. Soc. London. Series A, Mathematical and Physical Sciences 258 (1088), 145–167.

Wolfe, C.J., Solomon, S.C., Laske, G., Collins, J.A., Detrick, R.S., Orcutt, J.A., Bercovici, D., Hauri, E.H., 2009. Mantle shear-wave velocity structure beneath the Hawaiian hot spot. Science 326 (58–59), 1388–1390.

Xu, C., Huang, Z., Liu, C., Qi, I., Li, W., Guan, T., 2003. Geochemistry of carbonatites in Maoniuping REE deposit, Sichuan Province. Sci. China, Ser. D 46, 246–256.

Xu, C., Chakhmouradian, A., Taylor, R., Kynicky, J., Li, W., Song, W., Fletcher, I., 2014. Origin of carbonatites in the South Qinling orogen: Implications for crustal recycling and timing of collision between the South and North China blocks. Geochim. Cosmochim. Acta 143, 189–206.

Yarmolyuk, V.V., Kuzmin, M.N., Kozlovsky, A.M., 2013. Late Paleozoic – Early Mesozoic within-plate magmatism in North Asia: traps, rifts, giant batholiths, and the geodynamics of their origin. Petrology 21 (2), 101–126.

Zhao, D., 2004. Global tomographic images of mantle plumes and subducting slabs: insight into deep Earth dynamics. Phys. Earth Planet. Int. 146, 3–34.

Zonenshain, L.P., Kuzmin, M.N., 1983. Intraplate magmatism and its significance for understanding the processes in the Earth's mantle. Geotektonika 1, 28–45.

Zonenshain, L.P., Kuzmin, M.N., 1993. Paleogeodynamics [in Russian]. Nauka, Moscow.

Zonenshain, L.P., Kuzmin, M.N., Moralev V.M., 1976. Global Tectonics, Magmatism and Metallogeny [in Russian]. Nedra, Moscow.

Zonenshain, L.P., Kuzmin, M.I., Natapov, L.M., 1990. Geology of the USSR: A Plate Tectonic Synthesis, Geodyn. Ser., 21, Ed. B.M. Page, AGU, Washington, D.C.

Zorin, Yu.A., Turutanov, E. Kh., 2005. Plumes and geodynamics of the Baikal Rift Zone. Russian Geology and Geophysics (Geologiya i Geofizika) 46 (7), 669–682 (685–699).

Editorial responsibility: A.E. Izokh